Self-Immolative Carbamate Linkers for CD19-Budesonide Antibody-Drug Conjugates

Christopher C. Marvin*[a], Adrian D. Hobson[b], Michael McPherson[b], Theresa A. Dunstan[b], Thomas R. Vargo[b,c], Martin E. Hayes[b], Margaret M. Fettis[b], Agnieszka Bischoff[b], Lu Wang[b], Lu Wang[b], Axel Hernandez, Jr.[b], Ying Jia[b], Jason Z. Oh[b,c], Yu Tian[b]

[a] AbbVie Inc., 1 North Waukegan Road, North Chicago, IL 60064, United States

[b] AbbVie Bioresearch Center, 381 Plantation Street, Worcester, MA 01605, United States

[c] Former AbbVie Employee

Abstract

Antibody-drug conjugates consist of potent small molecule payloads linked to a targeting antibody. Payloads must possess a viable functional group by which a linker for conjugation can be attached. Linker-attachment options remain limited for connection to payloads via hydroxyl groups. A releasing group based on 2-aminopyridine was developed to enable stable attachment of *para*-aminobenzyl carbamate (PABC) linkers to the C21-hydroxyl group of budesonide, a glucocorticoid receptor agonist. Payload release involves a cascade of two self-immolative events that are initiated by protease-mediated cleavage of the dipeptide-PABC bond. Budesonide release rates were determined for a series of payload-linker intermediates in buffered solution at pH 7.4 and pH 5.4, leading to the identification of 2-aminopyridine as the preferred releasing group. Addition of a polyethylene glycol group improved linker hydrophilicity, thereby providing CD19-budesonide ADCs with suitable properties. **ADC23** demonstrated targeted budesonide delivery to CD19 expressing cells and inhibited B-cell activation in mice.

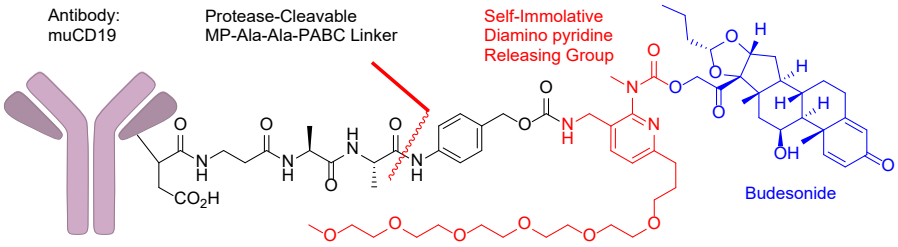

Key Words

Antibody-drug conjugates, budesonide, glucocorticoid receptor modulator, steroid, protease cleavable linker, self-immolative, CD19, targeted drug delivery

Introduction

Antibody-drug conjugates (ADC) are a growing class of pharmaceutical drugs that are designed to afford a targeted therapy. This approach combines a therapeutically active small molecule, often referred to as a payload,[1] with the cell-specific targeting of an antibody. These components are covalently connected to one another via a linker. There are currently eleven ADCs approved by the FDA in the United States with one additional ADC marketed exclusively in China. Five of these ADCs feature the auristatin payload, MMAE, conjugated via a linker composed of a dipeptide and a *para*-aminobenzyl carbamate (PABC), which attaches to the payload via a secondary amine (Fig. 1a). Protease-mediated cleavage of

the dipeptide triggers self-immolation of the PABC group and releases the small molecule payload.

We have been interested in the discovery and development of ADCs for autoimmune disease.[2,3] Glucocorticoids are potent small molecules that are well-established in the clinic for treatment of conditions such as rheumatoid arthritis, inflammatory bowel disease, psoriasis, polymyalgia rheumatica, lupus, and others. While effective, glucocorticoid use is limited by undesired side effects that are driven by on-target activity in non-diseased tissues. Since the glucocorticoid receptor is widely expressed in tissues such as bone, skin, gastrointestinal, and central nervous system tissues, we proposed that an ADC approach might provide targeted efficacy with mitigation of side effects through minimization of systemic glucocorticoid exposure. An important step toward this goal was the identification of an appropriate linker. The most validated linker technology, MC-Val-Ala-PABC, requires that the payload possess a nitrogen attachment site for carbamate formation (Fig. 1a). Our previous work involved development of novel ADC-specific glucocorticoid receptor modulators (GRMs) possessing an amine for linker attachment. Herein we describe an alternative approach, involving novel linker technology that enables conjugation and delivery of budesonide, a marketed GRM.

From a design perspective, we considered the direct application of PABC linkers with a budesonide payload as undesirable. Attachment of these linkers to budesonide via the C21-oxygen would result in the formation of a carbonate group. Carbonate prodrugs are known to have short plasma half-lives.[4] Although the ADC sacituzumab govitecan uses a carbonate linker to connect to its SN-38 payload, this carbonate is the weakest link in the conjugate. Hydrolysis in plasma leads to ~50% payload release in 18 hours after dosing.[5–7] Carbonate and ester linker strategies also were used to generate anti-CD163 ADCs with the GRM dexamethasone, which had a reported plasma half-life of 20 min in rats.[8–12] In this case, stability of the ADC was unclear, as this short half-life may be driven by rapid uptake of the CD163 antibody by the liver and spleen.[9] Nevertheless, we were concerned that the plasma stability of carbonate linkers could be limiting in comparison to carbamate-based linkers.

The most successful ADC approach for linker attachment to a payload via a hydroxyl group is exemplified by trastuzumab deruxtecan.[13,14] It consists of a HER2 antibody linked to its deruxtecan payload via a cleavable *N*-acyl-*N*,*O*-acetal. Another intriguing approach for hydroxy payloads involves pyrophosphate diesters and PABOH-phosphate esters.[15–17] Both phosphate-based linker technologies are plasma stable and involve two separate enzyme-mediated cleavage steps. The first enzymatic step generates a payload-phosphate. A second step involves phosphatase release of the active small molecule.

For a budesonide ADC, we placed a high value on the identification of a plasma stable linker due to the importance of limiting systemic exposure of non-conjugated payload to non-disease tissues. Furthermore, we prioritized linker designs that would be cleaved by action of a single enzymatic process. Linkers requiring multiple enzymatic steps for payload release were viewed as undesirable due to the prospect of additional complexity in the optimization of structure-activity relationships (SAR). Therefore, we proposed a novel linker possessing a second self-immolative linker group that would serve as a bridge between PABC and the GRM payload (Fig 1b). Our first design used amino benzylamine (ABA), which bridges PABC to an oxygen atom on the payload via a second, reversed, carbamate. Protease-mediated cleavage of ADC catabolite **2** was expected to give unstable PABC intermediate **3**, which would undergo self-immolation to **4**. ABA-containing intermediate **4** would then undergo cyclization to produce cyclic urea **5** and release budesonide (**6**). Related strategies involving diamine releasing groups have been reported for payload release. Most notably, an ethylene diamine group was used as a

bridging release group between PABOH and doucarmycin,[18] and in another case for sulfatase-triggered release of auristatin E.[19] A conceptually related pyrrolidine-carbamate self-immolative spacer recently was described for the release of camptothecin and resiquimod; however, it was not demonstrated in the context of an ADC.[20] Finally, we considered a third design criteria out of recognition of the fact that conjugation of hydrophobic linker-payloads to an antibody can result ADC aggregation. Aggregation may affect manufacturability, bioactivity, serum half-life, absorption rate and immunogenicity.[21] We expected that incorporation of hydrophilic moieties to the ABA group or its replacement with a heterocycle could mitigate aggregation if necessary and afford ADCs with appropriate properties.

An antibody recognizing mouse CD19 was selected due to the broad expression of CD19 on B-cells. CD19 is a surface expressed marker of B-cell development. It decreases the threshold of for antigen-dependent stimulation and is involved in downstream B-cell receptor signaling.[22–24] As such, it is recognized as a target for the treatment of autoimmune disorders as well as B-cell malignancies.

Figure 1. Proposed Linker Design.

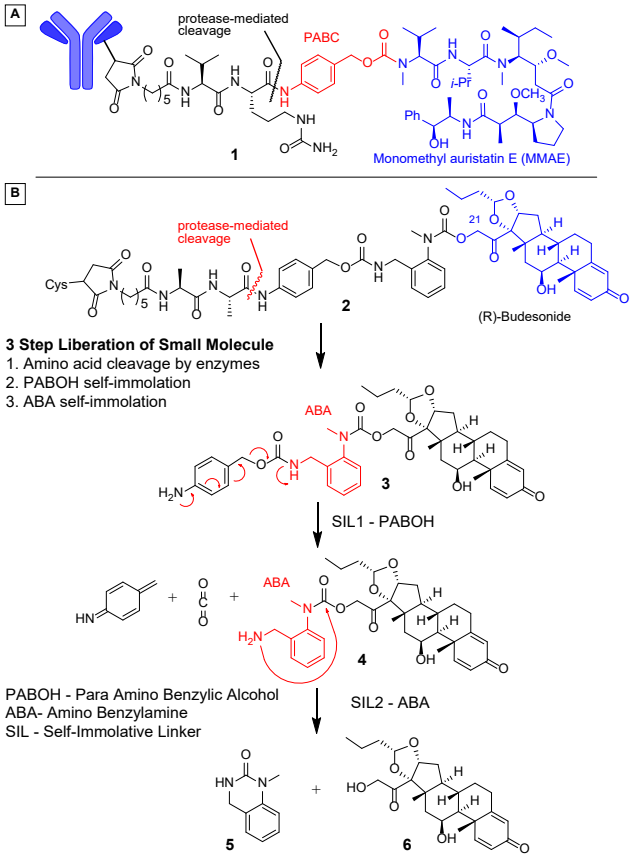

Results and Discussion

A set of Boc-protected aminomethylene-substituted anilines and aminopyridines were prepared for evaluation as releasing groups (Scheme 1). This set can be categorized into two subsets of compounds. The main series is the 2-amino benzylamine (ABA) series, represented by **RG-1**. A second subset involves compounds **RG-5** and **RG-6**, which were designed to decrease the lipophilicity of the releasing group.

The prototype ABA group, **RG-1**, was prepared by Raney nickel-catalyzed hydrogenation of commercially available benzonitrile **7** followed by selective Boc-protection. Several analogs that incorporate additional methyl groups were prepared with the expectation that these might offer rate enhancement for the self-immolative cyclization step (vide infra). **RG-2** introduces a single α-methyl at the benzylic position. This compound was prepared by SnAr reaction between 2-fluorobenzonitrile (**8**) and *N*-methylbenzylamine. Benzonitrile **9** then was reacted with methylmagnesium bromide, reduced with sodium borohydride and Boc-protected to form **10**. Hydrogenolysis of the benzyl protecting group completed **RG-2**. The related gem-dimethyl analog **RG-3** was prepared in one step from commercial **11**. A final analog in this benzene series, **RG-4**, was prepared through a SnAr addition of methylamine to **12**, followed by hydrogenation of the nitrile group and Boc protection of the primary amine.

Two isomeric pyridine-based releasing groups were prepared using similar methods. **RG-5** was prepared through a microwave-promoted SnAr reaction between **14** and methylamine, hydrogenation, and Boc protection. An isomeric pyridine, **RG-6**, was prepared in two steps from **16**.

Scheme 1. Release Group Synthesis.

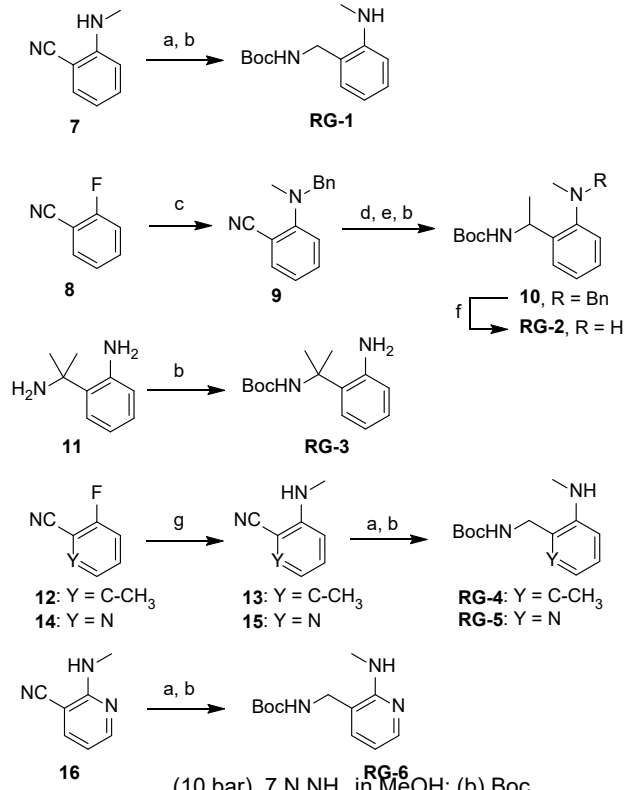

(a) Raney Ni, H_2 (10 bar), 7 N NH_3 in MeOH; (b) Boc_2O, Et_3N; (c) MeNHBn, DIPEA, NMP, 125 °C; (d) CH_3MgBr, THF, 50 °C; (e) $NaBH_4$, MeOH; (f) $Pd(OH)_2/C$, H_2 (10 bar), EtOH; (g) CH_3NH_2, MeOH, microwave.

Budesonide (**6**) was reacted with phosgene to give chloroformate **17** as a general intermediate for drug-linker synthesis (Scheme 2). The complete set of ABA and pyridine-based (APA) releasing group analogs were reacted in turn with this chloroformate to produce a series of Boc-protected carbamates represented by the general structure **18**. Conditions for Boc removal were carefully selected to avoid

premature cyclization and budesonide release. HCl in dioxane removes the protecting group and precipitates the resulting amine products as HCl salts (**Bud-RG**) in high purity.

Scheme 2. General Synthesis of Linker Fragments for Assessment of Steroid Release.

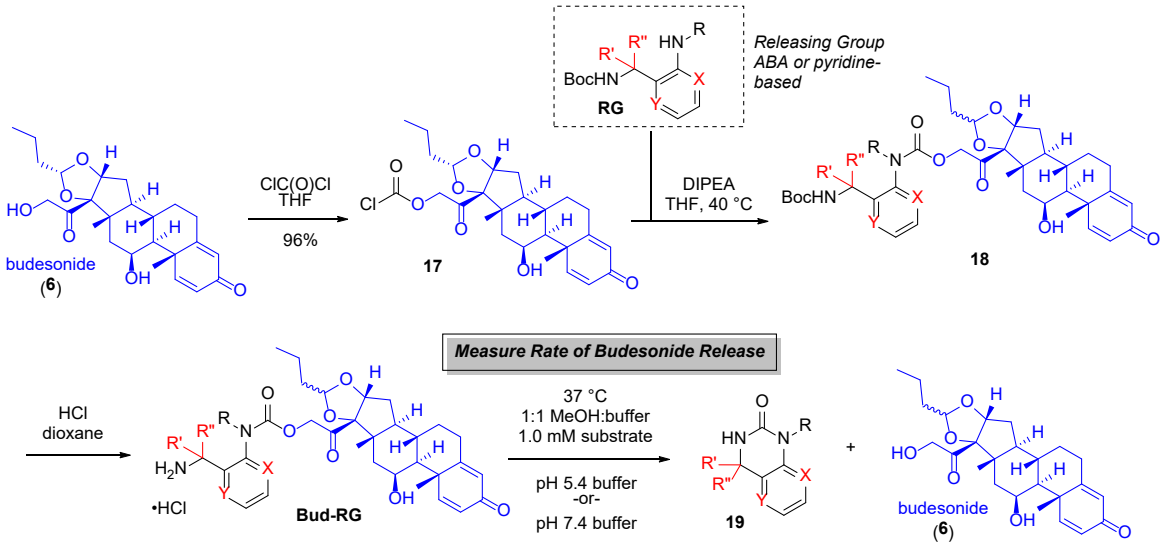

At this point, drug-linker intermediates **Bud-RG** were evaluated for their ability to release budesonide. Protease-mediated dipeptide cleavage and PABC immolation is understood to occur in the lysosome. While it was assumed that **Bud-RG** intermediates would be generated in the lysosome though catabolism of the corresponding ADCs, it was unclear whether **Bud-RG** compounds would liberate budesonide in the lysosome or cytosol. Therefore, HCl salts of **Bud-RG** were treated at 37 °C with pH 5.4 buffer to approximate conditions of the lysosome and then separately at the same temperature with a pH 7.4 buffer to approximate conditions of the cytoplasm. Formation of budesonide (**6**) and cyclic urea **19** were monitored by LCMS. Results for these experiments are summarized in Table 1, which presents relative rates as well as percent conversions at representative timepoints for additional context.

Table 1. Rates of Budesonide Release from Linker Intermediates at pH 5 and pH 7.

Releasing Group[a]	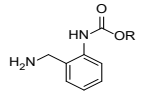 **Bud-RG-0**	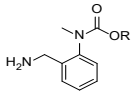 **Bud-RG-1**	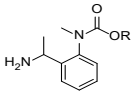 **Bud-RG-2**	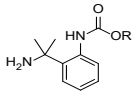 **Bud-RG-3**	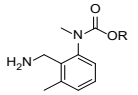 **Bud-RG-4**	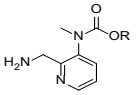 **Bud-RG-5**	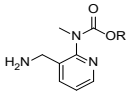 **Bud-RG-6**
Conversion[b], Time at pH 5.4	0%, 24 h	4%, 24 h	10%, 24 h	58%, 1 h	30% 24 h	0%, 72 h	80%, 3 h; 100%, 24 h
Relative Rate[b] at pH 5.4	NA[c]	1.125	2.75	523	1	NA[c]	112
Conversion[b], Time at pH 7.4	76%, 6 h;	76%, 16 h; 91%, 24 h	93%, 24 h	100%, 1 h	100%, 2h	9%, 72 h	100%, 1 h
Relative Rate[b] at pH 7.4	132	65	84	> 2978	121	1	> 3171

[a] Each of the releasing groups are connected to budesonide as represented by the "R" group.

[b] Percent conversions of the Bud-RG by LCMS at 37 °C. See supporting information for additional detail.

[c] NA = Not applicable. No conversion was observed in these entries.

Budesonide release was considerably more rapid at pH 7.4 in all cases as expected. As the baseline comparison, compound **Bud-RG-0** released no steroid at pH 5 after 24 h and 76% after 6 h at pH 7.

Introduction of methyl groups to the ABA core generally accelerated the rate of budesonide release. Significant rate enhancement was observed in the cases of **Bud-RG-3** and **Bud-RG-4**. Gem-dimethyl analog **Bud-RG-3** benefits from the Thorpe-Ingold effect, resulting in 58% release of budesonide within 1 h at pH 5.4. Similarly, the presence of an abutting methyl group on trisubstituted benzene **Bud-RG-4** drives cyclization through restriction of conformational freedom—an effect described as stereo-population control by Milstien and Cohen.[25–27]

Relative release rates for pyridine-based cores diverged dramatically. Pyridine **Bud-RG-5** was the poorest performing release group among these analogs. Only 9% conversion was observed after 72 h at pH 7.4 and none was observed at pH 5.4. In this case, it is plausible that an intramolecular hydrogen bond between the free amine and the proximal pyridine nitrogen locks this compound in an unreactive conformation. In contrast, isomer **Bud-RG-6** achieved 80% steroid release after only 3 h at pH 5.4. This was second only to the rate observed for gem-dimethyl releasing group **Bud-RG-3**. Based on these results, compounds that released measurable amounts of budesonide at pH 5.4 (**Bud-RG-1**, **Bud-RG-2**, **Bud-RG-3**, **Bud-RG-4**, and **Bud-RG-6**) were selected for elaboration to complete drug-linkers and conjugation as CD19 ADCs.

Conversion of the **Bud-RG** intermediates to full linkers was achieved convergently by the direct reaction of these HCl salts with *p*-nitrocarbonates represented by **20** in the presence of DIPEA (Scheme 3).[28,29] We chose to terminate our linkers in a standard maleimide caproamide (MC) conjugation group for screening purposes. This conjugation motif is prevalent in the ADC field, featuring prominently across FDA-approved ADC therapies, thereby providing a useful benchmark. Interestingly, we were unable to make an ADC with **Bud-RG-3**. This gem-dimethyl containing release group undergoes such rapid cyclization and steroid release that we could not engage it in an intermolecular coupling.

Scheme 3. General Synthetic Route to Drug-Linkers.

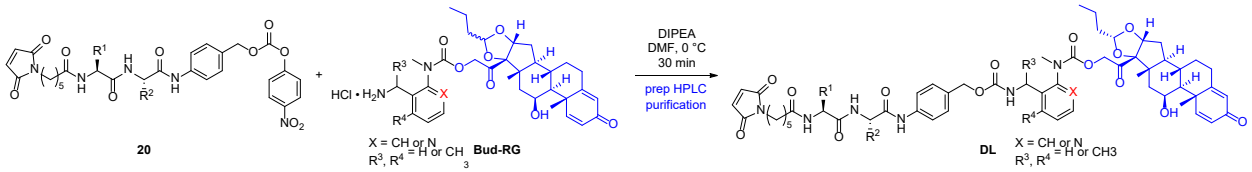

Mouse CD19 antibody was partially reduced with TCEP to reveal reactive cysteines and then conjugated through 1,4-addition to each maleimide drug-linker (**DL**). The resulting CD19-budesonide ADCs were characterized by size exclusion chromatography (SEC) to determine aggregation. Drug-to-antibody ratio (DAR) was determined by hydrophobic interaction chromatography (HIC) and mass spectrometry. ADCs were assessed for functional activity in a glucocorticoid response element (GRE) luciferase reporter assay in K562 cells that were engineered to express mu-CD19. Since wild-type K562 cells do not express CD19, targeted budesonide delivery by CD19 ADCs could be verified by comparison of GRE activity between CD19-knock in and non-specific uptake in wild type K562 cell lines. Table 2 summarizes the data for the resulting ADCs.

ADC1 with a linker featuring a standard Val-Cit dipeptide and release group **RG-1** provides a starting point for SAR comparisons (Table 2). In this case, conjugation to CD19 yielded only DAR2 and extremely high 40% aggregation due to hydrophobicity of the corresponding drug-linker (cLogP 4.90). While **ADC1** was active in the CD19-expressing GRE assay (EC_{50} = 2 µg/mL) the high level of aggregation was deemed unacceptable for further development. ADC aggregation has a detrimental effect on multiple drug-like

parameters. It increases non-specific cellular uptake and off-target toxicity due to FcγR activation and internalization[30,31] as well as poor PK in the form of rapid plasma clearance.[31–33]

We examined replacement of Val-Cit with other dipeptides to see if this portion of the linker could overcome the significant hydrophobicity imparted by the combination of a budesonide payload with a PABC linker and a benzene-based releasing group. Val-Ala linkers generally offer improved properties over Val-Cit even though cLogP suggests increased lipophilicity.[34,35] **ADC2** was indeed less aggregated by comparison. Moving to **ADC3** with an Ala-Ala dipeptide offered decreased aggregation at 24%, yet it offered no improvement with respect to GRE reporter activity.

It is noteworthy that it was possible to prepare **ADC3** with higher DAR loading compared to **ADC1** and **ADC2**. When comparing the aggregation levels, it is important to have similar DARs as this directly impacts aggregation. **ADC4** with Val-Glu provided approximately 30% aggregation across the **RG-1** releasing group series. It achieved the highest DAR loading across this series, offering improved GRE potency that was in line with higher DAR, and with 28-fold selectivity over the non-CD19 expressing cell line. Curiously, other more polar peptide combinations—Ser-Cit (**ADC5**), Asn-Cit (**ADC7**), Gln-Cit (**ADC8**)—did not improve ADC aggregation despite being less lipophilic compared to **ADC4**. The MC conjugation group itself contributes to hydrophobicity. Its replacement with the less lipophilic *N*-maleimidopropanamide (MP) offered no improvement despite its lower cLogP (compare **ADC6** with **ADC3**). Indeed, aggregation was consistently >30% for drug-linkers with lipophilicities below 3.5. Lower aggregation typically was observed with linker cLogPs ranging from 3.93-5.10 (**ADC3**, **ADC6**, and **ADC9**). This speaks to the complex interplay of additional parameters influencing ADC aggregation that are not accounted for by this single metric that does not account for contributions from the antibody. It is interesting that **ADC7** and **ADC8** were completely inactive in the reporter assay. This is consistent with data published elsewhere that indicates that linkers containing Asn-Cit and Gln-Cit are poor substrates for cathepsin-mediated release.[36]

The effect of the glucocorticoid payload on these properties was evaluated by replacing budesonide (cLogP 2.73) with triamcinolone acetonide (cLogP 1.94). **ADC9** had 20% aggregation at DAR3 and was less potent than the corresponding budesonide ADC, which was consistent with relative payload potency (see supporting information). We also replaced (*R*)-budesonide with (*S*)-budesonide, which is 20-fold less active the GRE reporter assay (See supporting information). Since ADCs would deliver budesonide to the acidic lysosome, we were curious whether acid-catalyzed epimerization of the acetal isomers might occur. We prepared **ADC10** with (*S*)-budesonide as a control and found that it was much less active in the CD19-expressing GRE reporter cell line (**ADC3**: EC_{50} = 3 μg/mL; **ADC10**: EC_{50} >20 μg/mL). These potency differences are consistent with the pure (R)- and (S)-payload activity, suggesting that minimal acetal epimerization occurs.

ADCs with the alternative releasing groups were examined. **ADC11** demonstrated that **RG-2** offered comparable GRE reporter activity to those ADCs with **RG-1**. The additional methyl groups on **RG-2** and **RG-3** that enhanced the release of budesonide in buffer had a negative effect on ADC aggregation. **ADC12** had 35% aggregation at DAR2 and was not tested in reporter assay as a result.

In contrast to the poor conjugate properties of the benzene-based (ABA) releasing groups, the aminopyridine-based (APA) releasing group, **RG-6**, dramatically reduced aggregation. **ADC13** has a pyridine-based releasing group with triamcinolone acetonide as the payload. We were encouraged by the low aggregation at DAR3 and especially intrigued by its improved GRE activity versus its direct comparator **ADC9**.

Table 2. Characterization of ADCs with ABA and APA Release Groups.

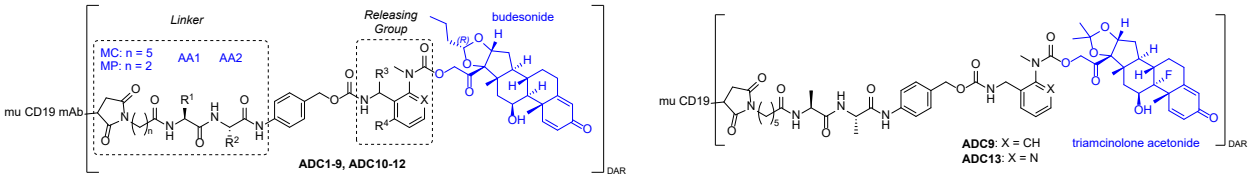

ADC	Linker	Releasing Group	Payload	DAR	Agg. (%)	Linker cLogP[a]	K562 CD19 GRE	K562 WT GRE
							EC_{50} (μg/mL)[b]	
ADC1	MC-Val-Cit	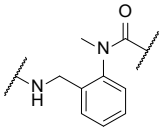 **RG-1**	(R)-Budesonide	2.1	43	4.90	2	ND[c]
ADC2	MC-Val-Ala		(R)-Budesonide	2.2	31	5.99	NV[d]	ND
ADC3	MC-Ala-Ala		(R)-Budesonide	2.6	24	5.10	3 (8)	20
ADC4	MC-Val-Glu		(R)-Budesonide	4.1	32	5.64	0.7 (2)	>20
ADC5	MC-Ser-Cit		(R)-Budesonide	2.7	31	2.97	NV[c]	ND
ADC6	MP-Ala-Ala		(R)-Budesonide	3	27	3.93	1.7	ND
ADC7	MP-Asn-Cit		(R)-Budesonide	3	37	1.39	>20	ND
ADC8	MP-Gln-Cit		(R)-Budesonide	3.1	38	1.68	>20	ND
ADC9	MC-Ala-Ala		Triamcinolone acetonide	2.9	21	4.31	5.6 (5)	ND
ADC10	MC-Ala-Ala		(S)-Budesonide	3	30	5.10	>20	ND
ADC11	MC-Val-Ala	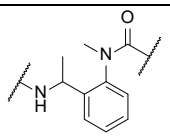 **RG-2**	(R)-Budesonide	2	35	6.41	1.6	ND
ADC12	MC-Ala-Ala	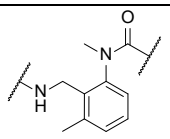 **RG-4**	(R)-Budesonide	3.3	33	5.62	ND	ND
ADC13	MC-Ala-Ala	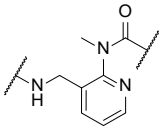 **RG-6**	Triamcinolone acetonide	3.9	1.5	3.69	1.3	ND

[a] AlogP and ChemAxon cLogP were calculated for the unconjugated maleimide drug-linkers.

[b] ADCs were tested as duplicates in the GRE reporter assay. Parentheses indicate the number of times the assay was repeated (each with an n=2) with data reported as the mean result.

[c] ND indicates not determined.

[d] NV indicates no value due to lack of differentiation compared to negative control.

We next turned our focus to the synthesis of second-generation releasing groups that modify ABA (**RG-1**) and APA (**RG-6**) through incorporation of additional hydrophilic solubilizing groups (Scheme 4a). Two sites were chosen for modification: (1) addition of polyethylene glycol (PEG) units to the aromatic ring, and (2) modification of the *N*-methyl group to introduce polar functional groups. Briefly, synthesis involved PEG introduction via Sonogashira coupling of an aryl halide **21** with the appropriate propargylic PEG

intermediate **22**. Hydrogenation of the alkyne and then nitrile groups provided a benzylic amine, which was Boc-protected to give releasing group intermediates **24a-c**.

Scheme 4. Synthesis of 2nd Generation Release Groups for Improved Solubility.

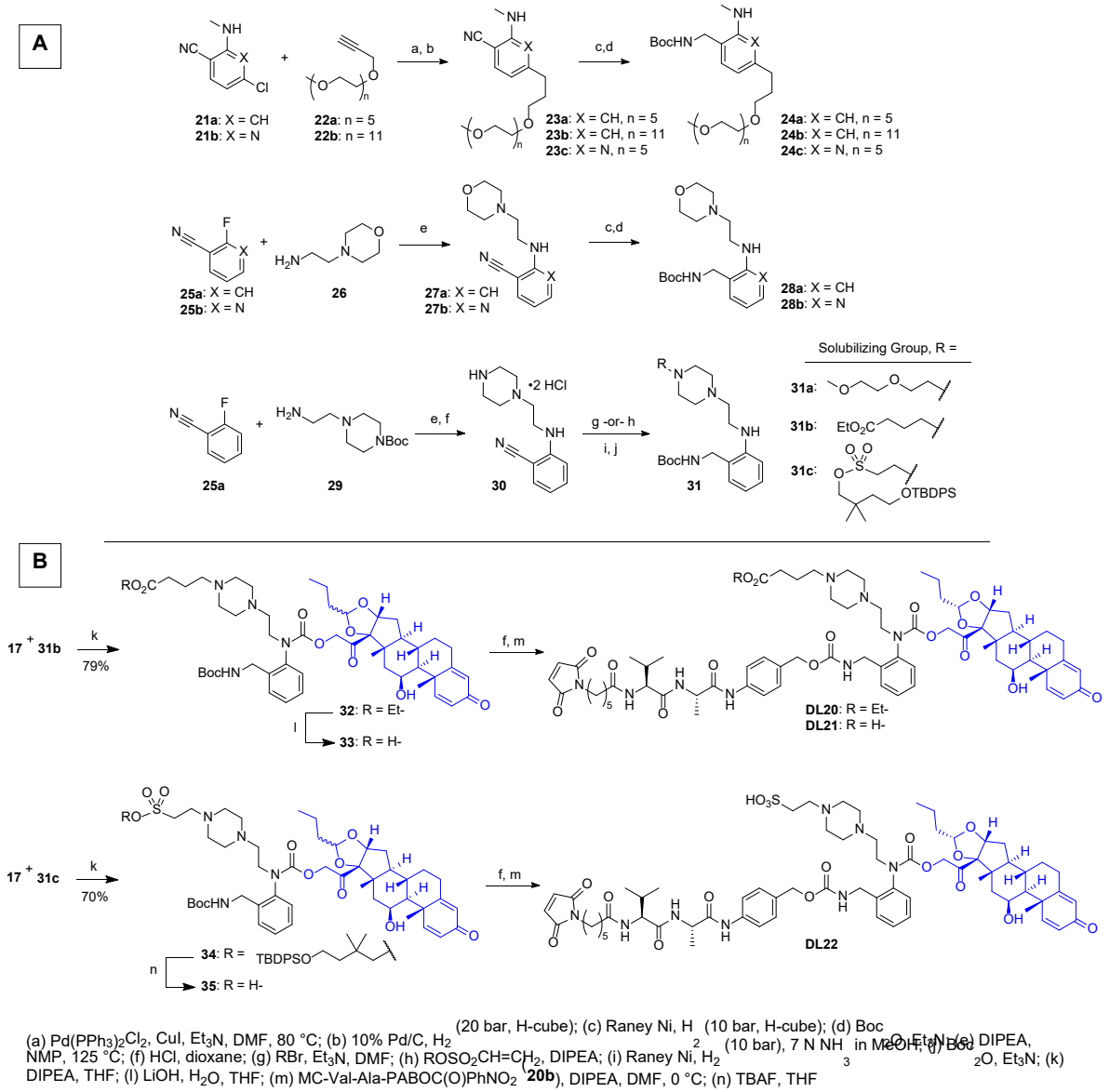

(a) $Pd(PPh_3)_2Cl_2$, CuI, Et_3N, DMF, 80 °C; (b) 10% Pd/C, H_2 (20 bar, H-cube); (c) Raney Ni, H_2 (10 bar, H-cube); (d) Boc$_2$O, Et_3N; (e) DIPEA, NMP, 125 °C; (f) HCl, dioxane; (g) RBr, Et_3N, DMF; (h) $ROSO_2CH{=}CH_2$, DIPEA; (i) Raney Ni, H_2 (10 bar), 7 N NH_3 in MeOH; (j) Boc$_2$O, Et_3N; (k) DIPEA, THF; (l) LiOH, H_2O, THF; (m) MC-Val-Ala-PABOC(O)PhNO$_2$ (**20b**), DIPEA, DMF, 0 °C; (n) TBAF, THF

Solubilizing groups on the aryl nitrogen were introduced via SnAr reaction between an aryl fluoride **25** with aminoethyl morpholine **26** or aminoethylpiperazine **29**. After Boc-deprotection, piperazine intermediate **30** was diversified through alkylation of the secondary amine with alkyl bromides to give PEG (**31a**) and ethyl butyrate analogs (**31b**). Alternatively, **30** could be alkylated through 1,4-addition to an unsaturated sulfonate ester to give **31c**.[37] For all examples, nitrile reduction and Boc protection completed synthesis of releasing groups **31a-c**, which were ready for elaboration to the full drug-linkers. Drug-linker synthesis for most compounds proceeded via the general route shown previously in Scheme 3. Drug-linkers **DL21** and **DL22** with substituted piperazines required additional steps for the deprotection of the carboxylic and sulfonic acid groups (Scheme 4b).

Table 3 summarizes data for CD19 ADCs with the second-generation drug-linkers. The PEG6-functionalized benzene linker conjugated poorly and offered no improvement over the first-generation ABA releasing group ADCs (Table 3, **ADC14**). Extension of the sidechain from PEG6 to PEG12 decreased aggregation and, more impressively, improved GRE potency (**ADC15**, EC_{50} 0.20 µg/mL). Combination of PEG6 with an aminopyridine-based releasing group provided **ADC16** with excellent physical properties and an EC_{50} of 0.15 µg/mL for the reporter assay in target-expressing cells. Again, it is important to compare the DAR loadings when comparing ADC activity. Activity differences for **ADC15** versus **ADC16** are consistent with DAR. Activity differences in the non-target expressing cell lines may reflect differences in carbamate stability, suggesting that **ADC16** may release low levels of budesonide in the assay medium. Regardless, the 70-fold difference in activity between cell lines for **ADC16** supports targeted delivery as the predominant pathway.

Morpholine-based modification enabled conjugation to DAR4 (**ADC17** and **ADC18**). The aminopyridine-based drug-linker again decreased hydrophobicity, which gave a measurable improvement in aggregation for **ADC18**. However, these ADCs were less potent in GRE compared to **ADC16** (EC_{50} >1.2 µg/mL).

Although aggregation was < 10% for piperazine-based **ADC19-22**, their conjugation efficiency was generally poor with relatively low DAR. Furthermore, **ADC19-22** were similar to **ADC17** and **ADC18** with respect to their activity in the GRE reporter assay, with EC50s of 1.2-5.1 µg/mL. This suggests that introduction of a solubilizing group to the nitrogen of the *N*-aryl carbamate detrimentally affects release of budesonide from these ADCs.

The PEG6-aminopyridine release group (**RG-9**) was prioritized for follow-up based on the relatively low aggregation and promising reporter activity for **ADC16**. In preparation for in vivo assessment, two additional changes were made to optimize the drug-linker: (1) the maleimidocaproamide (MC) conjugation moiety was replaced with maleimidopropionamide (MP), and (2) the Val-Ala dipeptide was replaced with Ala-Ala. Both changes were made to further decrease the hydrophobicity of the drug-linker. Replacement of MC with the shorter MP group has an additional benefit as it renders the imide more susceptible to ring-opening by hydrolysis. 1,4-Addition of cysteine to MC terminated linkers is reversible. In plasma, maleimide is regenerated through elimination and then is exchanged with reactive cysteine species.[38,39] Imide hydrolysis decreases the reversibility of maleimide conjugations, blocking linker exchange and improving in vivo ADC stability.[40–42]

ADC23 was prepared using the MP-Ala-Ala modified linker and succinimide ring was hydrolyzed after conjugation for more stable attachment. Mean potency was similar to the MC-Val-Ala version (**ADC23** EC_{50} = 0.23 µg/mL; **ADC16** EC_{50} = 0.15 µg/mL). The matched isotype control, **ADC24** (tetX), had comparable DAR and was inactive on both GRE reporter cell lines as expected. This provides further support for CD19-targeted delivery of budesonide by **ADC23**.

Table 3. Characterization of ADCs with 2nd Generation Solubilizing Release Group Linkers.

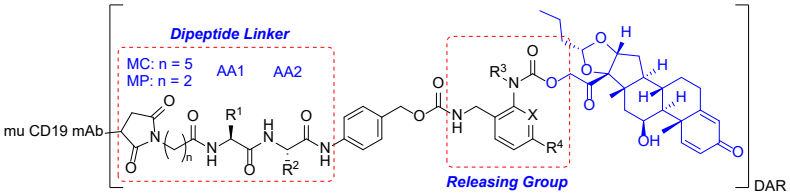

ADC	Linker	Releasing Group		DAR	Agg. (%)	cLogP	K562 CD19 GRE	K562 WT GRE
							EC_{50} (µg/mL)[a]	
ADC14	MC-Val-Cit	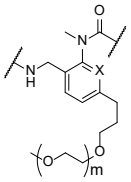	X = CH, PEG6 **RG-7**	2.4	28	6.37	ND[c]	ND
ADC15	MC-Val-Ala		X = CH, PEG12 **RG-8**	3.1	12	6.08	0.20	>20
ADC16	MC-Val-Ala		X = N, PEG6 **RG-9**	3.4	4.7	5.62	0.15 (3)[a]	11.5
ADC17	MC-Val-Cit	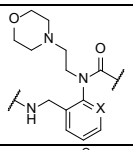	X = CH **RG-10**	4.3	15	4.70	1.2	ND
ADC18	MC-Val-Cit		X =N **RG-11**	4.3	7	4.08	3	ND
ADC19	MC-Val-Ala	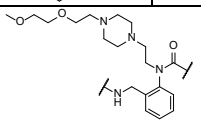 **RG-12**		2.2	7.5	5.76	3.4	ND
ADC20	MC-Val-Ala	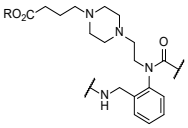	R = Et **RG-13**	2.3	8.5	6.36	3.4	ND
ADC21	MC-Val-Ala		R = H **RG-14**	2.8	6.5	3.15	1.2	ND
ADC22	MC-Val-Ala	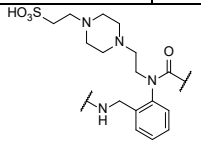 **RG-15**		2.3	2	3.40	5.1	ND
ADC23	MP-Ala-Ala	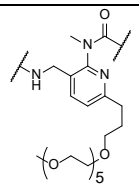 **RG-9**		4.3	2.6	3.55	0.23 (2)[a]	10 (2)[a]
ADC24[b]	MP-Ala-Ala			4.0	1.1	3.55	>20 (3)[a]	>20 (3)[a]

[a] ADCs were tested as duplicates in the GRE reporter assay. Parentheses indicate the number of times the assay was repeated (each with an n=2) with data reported as the mean result.

[b] Non-targeting isotype (anti-tetX) antibody ADC.

[c] ND indicates not determined.

We recently published results for α-TNF-ADCs featuring novel mono-aryl GRM payloads that do not require customized linker technology.[2] For comparison with those results, the optimized **RG-9** linker with budesonide was conjugated to mouse α-TNF. **ADC25** was then tested in the reporter assay, this time in a K562 cell line engineered to express mouse α-TNF (Table 4). In vitro activity for **ADC25** was similar to what had been observed for **ADC26** in the TNF-expressing cell line, whereas **ADC25** had more significant activity in the wild-type cell line. While antigen-targeted delivery predominates, the consistent activity of approximately 10 µg/mL in non-antigen expressing cells for aminopyridine linked ADCs (**ADC16**, **ADC23**, and **ADC25**) could be due to low levels of extracellular payload release in the cell media during the GRE assay. In the case of **ADC25**, increased non-specific uptake due to aggregation may also play a role. **ADC26** and its matched isotype, which do not have carbamate linkers, did not demonstrate any non-specific activity.

Table 4. Comparison of In Vitro Potency for Mouse α-TNF ADCs 25 and 26 and Isotype ADC 27.

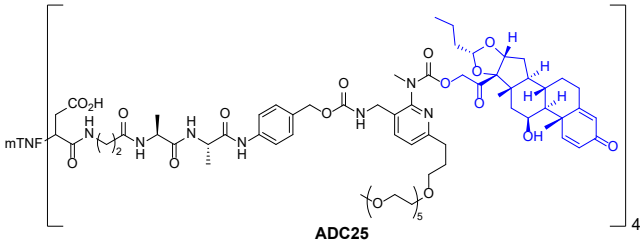

ADC25

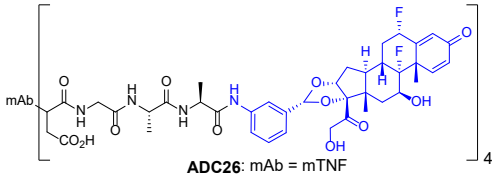

ADC26: mAb = mTNF
ADC27: mAb = OVA isotype

ADC	Antibody	DAR	Agg. (%)	K562 mTNF GRE	K562 WT GRE
				EC_{50} (µg/mL)	
ADC25	α-TNF	4.9	19.6	0.10	8.53
ADC26[a]	α-TNF	4.0	3.7	0.12	>50
ADC27[a]	α-OVA isotype	4.0	1.9	>50	>50

[a] See reference 2. OVA = ovalbumin.

ADC Stability

ADC16 and **ADC23** were profiled for stability in PBS buffer and plasma (see Supporting Information). Both were stable in buffer with no change observed by mass spectrometry over 7 days. **ADC16** with the MC-Val-Ala linker lost 2.4% drug-linker over 7 days in mouse plasma. In contrast, no loss of budesonide or linker was observed for **ADC23** under the same conditions in mouse, rat, or cynomolgus monkey plasma (Supporting Information). It was noted that budesonide alone has poor stability in plasma (mouse, rat, monkey) with < 10% remaining after 7 days in these matrixes.

In Vivo

CD19 is a transmembrane surface protein expressed across all B-cell lineages. It is involved in the B-cell antigen response and is a biomarker for the diagnosis and treatment of lymphomas. Efficacy of the CD19 ADCs was evaluated in a model where mice were immunized with NP-CGG (4-hydroxy-3 nitrophenylacetyl hapten-chicken Gamma Globulin). Exposure to this immunogen stimulates the formation of mature germinal centers (GC) wherein B-cells undergo proliferation and differentiation into activated lineages.[43] Development of activated GC B-cells with high affinity, antigen-specific, antibodies occurs within 10 days of immunization. It is established that glucocorticoid treatment suppresses B-cell proliferation, differentiation, and IgG production.[44–47] Therefore, immunization on day 0 was followed by i.p. dosing of the CD19-budesonide ADC on days 4, 6, 8, and 9. Spleens were collected 24 h after the last dose and processed for analysis by fluorescence activated cell sorting (FACS). Activated B-cells were defined by positive expression of B220 and low expression of IgD.

Loss of CD19+ B-cells was observed in groups treated with the unfunctionalized CD19 antibody and targeted **ADC23** (Fig. 2, left panel). CD19+ cell counts were not affected in any of the other groups. It is unclear whether low CD19+ cell counts in these two groups are due to competitive binding with extracellular CD19 antibody/ADC, or whether it is due to receptor internalization in these two treatment groups. Targeted **ADC23** decreased activated B-cell counts below vehicle levels, separating from the group treated with non-targeted isotype **ADC24** (Fig. 2, right panel). The CD19-budesonide ADC suppressed B-cell activation to levels that were similar to, although not as potent, as budesonide alone. This study validates the proof-of-concept for targeted delivery of budesonide by CD19-targeted ADC in an immunized mouse model.

Figure 2. Activity of ADC23 on B-cell Activation in Immunized Mice

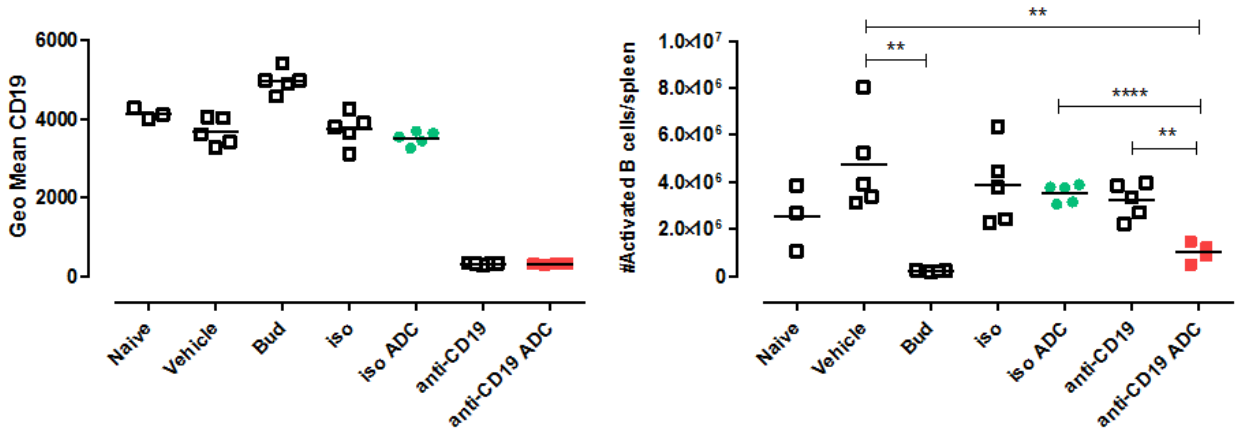

Figure 2 Caption: Five female C57BL.6N mice per group were immunized on day 0 with NP-CGG. On days 4, 6, 8, and 9 they were dosed i.p. according to the following: (A) naïve = non-immunized group; no treatment; (B) vehicle = (DPBS), (C) bud = budesonide (10 mg/kg), (D) iso = anti-tetX (30 mg/kg), (E) iso ADC = anti-tetX-budesonide ADC, **ADC24** (30 mg/kg), (F) anti-CD19 = muCD19 antibody (30 mg/kg), (G) anti-CD19 ADC = muCD19 antibody-budesonide ADC, **ADC23** (30 mg/kg).

Summary and Conclusions

We identified novel carbamate releasing groups that bridge protease cleavable PABC linkers for attachment to payloads via hydroxy groups. This was demonstrated in the context of a CD19-targeted

antibody that selectively delivers budesonide to antigen-expressing cells. 2-Aminopyridine (**RG-6**, **RG-9**) was identified as a promising release group motif based on comparison of release kinetics for a panel of diamino release groups in buffers that modeled the pH of the lysosome and cytosol. Appending standard MC-Val-Cit-PABC linkers to these release groups and conjugation to muCD19 antibodies generated ADCs with relatively poor physical chemical properties as evidenced by high aggregation. Although linker modification with less hydrophobic dipeptides only modestly improved ADC aggregation, more significant property improvement was achieved by addition of solubilizing groups. PEG-functionalized pyridine linkers enabled reproducible preparation of DAR4 ADCs that achieved EC_{50}'s of less than 1 µg/mL in an in vitro GRE reporter assay. Selectivity of >40-fold was achieved for selective budesonide delivery to engineered antigen expressing K562 cells over wild-type cells. **ADC23** was active in an immunized mouse model where suppression of B-cell activation was observed. In this model, the CD19-targeted ADC showed greater activity than matched isotype and achieved similar levels of activity to the small molecule alone. This work establishes that budesonide can be delivered by a CD19 ADC using a novel carbamate linker. Further work from our lab in the area of glucocorticoid ADCs will be reported in due course.

Experimental

All the reagents and solvents were purchased from Combi-Blocks, MilliporeSigma, BroadPharm, Chem-Impex, Goldenbridge, or other vendors as noted, and used without further purification. Reactions were carried out under an inert atmosphere of nitrogen. Yields refer to isolated yields of analytically pure (>95%) material unless noted otherwise. Compound names were generated with Perkin Elmer ChemDraw 20.1. Whenever possible reactions were monitored by LCMS. All purified compounds were ≥95% purity based on analytical HPLC. HPLC conditions are detailed in Table SI-2 in the Supporting Information. Magnetic resonance spectra (^{1}H and ^{13}C NMR) were measured with either a 400, 500, or 600 MHz spectrometer. NMR data were processed with MestReNova software. Chemical shifts are reported in parts per million (δ, ppm). First order splitting patterns were interpreted and coupling constants rounded to the nearest 0.1 Hz. Splitting patterns are designated as: s, singlet; d, doublet; t, triplet; q, quartet; m, multiplet; and comp, overlapping multiplets of non-magnetically equivalent protons. ^{1}H NMR spectra are referenced to residual chloroform (7.27 ppm) or residual dimethyl sulfoxide (2.50 ppm); ^{13}C NMR spectra are referenced to the central line of the 1:1:1 triplet of $CDCl_3$ (77.23 ppm) or DMSO-d6 (39.52 ppm).

Synthesis Procedures

2-((6aR,6bS,7S,8aS,8bS,11aR,12aS,12bS)-7-Hydroxy-6a,8a-dimethyl-4-oxo-10-propyl-2,4,6a,6b,7,8,8a,8b,11a,12,12a,12b-dodecahydro-1H-naphtho[2',1':4,5]indeno[1,2-d][1,3]dioxol-8b-yl)-2-oxoethyl carbonochloridate (17)

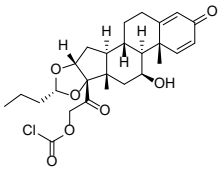

Phosgene (20 wt% in toluene, 9.8 mL, 18.58 mmol) was added to a solution of (6aR,6bS,7S,8aS,8bS,10R,11aR,12aS,12bS)-7-hydroxy-8b-(2-hydroxyacetyl)-6a,8a-dimethyl-10-propyl-6a,6b,7,8,8a,8b,11a,12,12a,12b-decahydro-1H-naphtho[2',1':4,5]indeno[1,2-d][1,3]dioxol-4(2H)-one (*R*-

budesonide, **6**) (2.0 g, 4.65 mmol) in THF (46.5 mL). A diffusing bubbler was added to the outlet of the nitrogen side of the Schlenk line, containing a saturated aqueous solution of sodium bicarbonate to quench any escaping phosgene. The reaction was allowed to stir at room temperature for 2 h. Solvent was removed under reduced pressure and then the residue was dried under high vacuum. 2-((6aR,6bS,7S,8aS,8bS,11aR,12aS,12bS)-7-Hydroxy-6a,8a-dimethyl-4-oxo-10-propyl-2,4,6a,6b,7,8,8a,8b,11a,12,12a,12b-dodecahydro-1H-naphtho[2',1':4,5]indeno[1,2-d][1,3]dioxol-8b-yl)-2-oxoethyl carbonochloridate (**17**) (2.29g, 96% yield) was isolated as a crystalline solid, which was used in the subsequent reaction without further purification. LCMS (Table SI-2, Method f) Rt = 1.83 min; m/z 493.1 [M+H$^+$].

6-(2,5,8,11,14,17-Hexaoxaicosan-20-yl)-2-(methylamino)nicotinonitrile (23c)

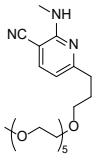

Step 1, General Procedure for Sonogashira Coupling: Bis(triphenylphosphine) Pd (II) dichloride (0.043 g, 0.061 mmol), copper(I) iodide (5.77 mg, 0.030 mmol), and triethylamine (0.34 mL, 2.422 mmol) were added to a degassed solution of 6-chloro-2-(methylamino)nicotinonitrile (**21b**) (0.203 g, 1.211 mmol) and 2,5,8,11,14,17-hexaoxaicos-19-yne (**22a**) (0.457 g, 1.575 mmol) in DMF (4.84 mL). The reaction mixture was heated to 80 °C for 5 h. Charged with more Bis(triphenylphosphine) Pd (II) dichloride (0.043 g, 0.061 mmol) and copper(I) iodide (5.77 mg, 0.030 mmol) and 2,5,8,11,14,17-hexaoxaicos-19-yne (**22a**) (0.1 g, 0.34 mmol). Continued heating at 80 °C with stirring overnight. Cooled to room temperature and removed solvent under reduced pressure. Purification by chromatography (silica) eluting with a gradient of 0-10% MeOH/DCM to give 6-(2,5,8,11,14,17-hexaoxaicos-19-yn-20-yl)-2-(methylamino)nicotinonitrile (0.210 g, 41% yield) as a dark yellow residue, which was dried under high vacuum. ^{1}H NMR (400 MHz, DMSO-*d*6) δ 7.90 (d, *J* = 7.7 Hz, 1H), 7.23 (d, *J* = 4.6 Hz, 1H), 6.76 (d, *J* = 7.7 Hz, 1H), 4.44 (s, 2H), 3.66 – 3.60 (m, 2H), 3.60 – 3.55 (m, 2H), 3.55 – 3.45 (m, 14H), 3.45 – 3.38 (m, 2H), 3.23 (s, 3H), 2.83 (d, *J* = 4.6 Hz, 3H). LCMS (Table SI-2, Method b) R_t = 1.81 min.; m/z = 422.4 [M+H$^+$].

Step 2, General Procedure for Alkyne Hydrogenation: A solution of 6-(2,5,8,11,14,17-hexaoxaicos-19-yn-20-yl)-2-(methylamino)nicotinonitrile (0.210 g, 0.498 mmol) in ethanol (5 mL) was passed through H-Cube at 1mL/min over 10% Pd/C cartridge and 10 bar hydrogen for 90 minutes. Concentrated under reduced pressure to give 6-(2,5,8,11,14,17-hexaoxaicosan-20-yl)-2-(methylamino)nicotinonitrile (**23c**) (0.177 g, 83% yield) was obtained as a light yellow oil. LCMS (Table SI-2, Method b) R_t = 1.88 min.; m/z = 426.4 [M+H$^+$]. light yellow oil. LCMS (Table SI-2, Method b) R_t = 1.88 min.; m/z = 426.4 [M+H$^+$].

tert-Butyl ((6-(2,5,8,11,14,17-hexaoxaicosan-20-yl)-2-(methylamino)pyridin-3-yl)methyl)carbamate (24c)

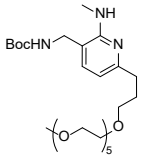

Step 1, General Procedure for Nitrile Hydrogenation: A solution of 6-(2,5,8,11,14,17-hexaoxaicosan-20-yl)-2-(methylamino)nicotinonitrile (**23c**) (0.177 g, 0.416 mmol) in 7 N NH_3 in MeOH (4.2 mL) was passed

through H-Cube at 1 mL/min over Raney Ni cartridge and 10 bar hydrogen for 90 min. Solvent was removed under reduced pressure to give 3-(aminomethyl)-6-(2,5,8,11,14,17-hexaoxaicosan-20-yl)-*N*-methylpyridin-2-amine (0.127 g, 71% yield) as a yellow oil. ^{1}H NMR (400 MHz, DMSO-d6) δ 7.19 (d, J = 7.2 Hz, 1H), 6.39 (d, J = 5.5 Hz, 1H), 6.33 (d, J = 7.2 Hz, 1H), 3.60 (s, 2H), 3.55 - 3.45 (m, 18H), 3.45 - 3.38 (m, 4H), 3.23 (s, 3H), 2.83 (d, J = 4.3 Hz, 3H), 2.55 (dd, J = 8.5, 6.7 Hz, 2H), 1.86 (dt, J = 8.7, 6.7 Hz, 2H). LCMS (Table SI-2, Method b) R_t = 1.05 min.; m/z = 430 [M+H$^+$].

Step 2, General Procedure for Boc-Protection: Triethylamine (0.045 mL, 0.325 mmol) followed by Boc_2O (0.072 mL, 0.310 mmol) were added to a solution of 3-(aminomethyl)-6-(2,5,8,11,14,17-hexaoxaicosan-20-yl)-*N*-methylpyridin-2-amine (0.127 g, 0.296 mmol) in ACN (3 mL). After the reaction was complete, solvent was removed under reduced pressure. Purification by chromatography (silica) eluting with a gradient of 60-100% EtOAc/heptane gave tert-Butyl ((6-(2,5,8,11,14,17-hexaoxaicosan-20-yl)-2-(methylamino)pyridin-3-yl)methyl)carbamate (**24c**) (0.127 g, 81% yield) as an orange oil that was dried in the vacuum oven. ^{1}H NMR (400 MHz, DMSO-d6) δ 7.24 (d, J = 6.5 Hz, 1H), 7.09 (d, J = 7.2 Hz, 1H), 6.33 (d, J = 7.4 Hz, 1H), 5.90 (s, 1H), 3.89 (d, J = 6.2 Hz, 2H), 3.54 - 3.45 (m, 18H), 3.44 - 3.39 (m, 4H), 2.83 (d, J = 4.5 Hz, 3H), 2.54 (dd, J = 8.5, 6.7 Hz, 2H), 1.85 (dq, J = 8.9, 6.6 Hz, 2H), 1.39 (s, 9H). LCMS (Table SI-2, Method b) R_t = 1.69 min; m/z = 530.3 [M+H$^+$].

2-((6aR,6bS,7S,8aS,8bS,10R,11aR,12aS,12bS)-7-Hydroxy-6a,8a-dimethyl-4-oxo-10-propyl-2,4,6a,6b,7,8,8a,8b,11a,12,12a,12b-dodecahydro-1H-naphtho[2',1':4,5]indeno[1,2-d][1,3]dioxol-8b-yl)-2-oxoethyl (3-(((*tert*-butoxycarbonyl)amino)methyl)-6-(2,5,8,11,14,17-hexaoxaicosan-20-yl)pyridin-2-yl)(methyl)carbamate (Bud-RG-9-Boc)

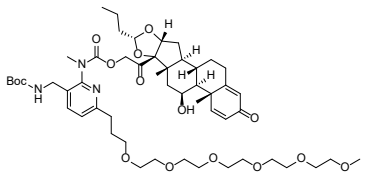

Sequentially, DIPEA (0.08 mL, 0.453 mmol) followed by a suspension of *tert*-butyl ((6-(2,5,8,11,14,17-hexaoxaicosan-20-yl)-2-(methylamino)pyridin-3-yl)methyl)carbamate (**24c**) (0.08 g, 0.151 mmol) in THF (0.56 mL) were added to a solution of 2-((6aR,6bS,7S,8aS,8bS,10R,11aR,12aS,12bS)-7-hydroxy-6a,8a-dimethyl-4-oxo-10-propyl-2,4,6a,6b,7,8,8a,8b,11a,12,12a,12b-dodecahydro-1H-naphtho[2',1':4,5]indeno[1,2-d][1,3]dioxol-8b-yl)-2-oxoethyl carbonochloridate (**17**) (0.082 g, 0.166 mmol) in THF (1.1 mL). The reaction was heated to 40 °C and stirred for 7 h, whereupon a second portion of **17** (40 mg, 0.081 mmol) was added and heating continued at 40 °C overnight. A third charge of **17** (20 mg, 0.0405 mmol) was added and heating continued for an additional 2 h. Removed solvent under reduced pressure. Purification by chromatography (silica) eluting with a gradient of 0-100% EtOAc/heptane, then 0-10% MeOH/DCM gave 2-((6aR,6bS,7S,8aS,8bS,10R,11aR,12aS,12bS)-7-hydroxy-6a,8a-dimethyl-4-oxo-10-propyl-2,4,6a,6b,7,8,8a,8b,11a,12,12a,12b-dodecahydro-1H-naphtho[2',1':4,5]indeno[1,2-d][1,3]dioxol-8b-yl)-2-oxoethyl (3-(((tert-butoxycarbonyl)amino)methyl)-6-(2,5,8,11,14,17-hexaoxaicosan-20-yl)pyridin-2-yl)(methyl)carbamate (**Bud-RG-9-Boc**) (0.113 g, 76% yield) as an orange oil that became a foam after drying under high vacuum. LCMS (Table SI-2, Method b) R_t = 2.63 min.; m/z = 1003 [M+NH_4^+].

2-((6aR,6bS,7S,8aS,8bS,10R,11aR,12aS,12bS)-7-Hydroxy-6a,8a-dimethyl-4-oxo-10-propyl-2,4,6a,6b,7,8,8a,8b,11a,12,12a,12b-dodecahydro-1H-naphtho[2',1':4,5]indeno[1,2-d][1,3]dioxol-8b-yl)-2-oxoethyl (3-(aminomethyl)-6-(2,5,8,11,14,17-hexaoxaicosan-20-yl)pyridin-2-yl)(methyl)carbamate hydrochloride (Bud-RG-9)

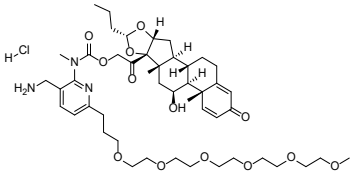

A 4.0 M solution of HCl in dioxane (0.3 mL, 1.146 mmol) was added to a solution of 2-((6aR,6bS,7S,8aS,8bS,10R,11aR,12aS,12bS)-7-hydroxy-6a,8a-dimethyl-4-oxo-10-propyl-2,4,6a,6b,7,8,8a,8b,11a,12,12a,12b-dodecahydro-1H-naphtho[2',1':4,5]indeno[1,2-d][1,3]dioxol-8b-yl)-2-oxoethyl (3-(((tert-butoxycarbonyl)amino)methyl)-6-(2,5,8,11,14,17-hexaoxaicosan-20-yl)pyridin-2-yl)(methyl)carbamate (**Bud-RG-9-Boc**) (0.113 g, 0.115 mmol) in dioxane (1.146 mL). The reaction was stirred at room temperature for 16 h. Solvent was removed under reduced pressure. The residue was triturated with ether and sonicated. The solid was filtered and dried solid in vacuum oven at 60 °C for 1 h to give 2-((6aR,6bS,7S,8aS,8bS,10R,11aR,12aS,12bS)-7-hydroxy-6a,8a-dimethyl-4-oxo-10-propyl-2,4,6a,6b,7,8,8a,8b,11a,12,12a,12b-dodecahydro-1H-naphtho[2',1':4,5]indeno[1,2-d][1,3]dioxol-8b-yl)-2-oxoethyl (3-(aminomethyl)-6-(2,5,8,11,14,17-hexaoxaicosan-20-yl)pyridin-2-yl)(methyl)carbamate hydrochloride (**Bud-RG-9**) (0.0886 g, 81% yield). ^{1}H NMR (400 MHz, DMSO-*d*6) δ 8.26 (s, 4H), 7.96 (s, 1H), 7.33 (dd, *J* = 18.5, 9.0 Hz, 2H), 6.15 (dd, *J* = 10.1, 1.9 Hz, 1H), 5.91 (d, *J* = 1.4 Hz, 1H), 4.80 (d, *J* = 26.2 Hz, 3H), 4.69 (s, 1H), 4.63 (s, 1H), 4.08 (d, *J* = 168.8 Hz, 4H), 3.54 – 3.41 (m, 19H), 3.44 – 3.37 (m, 3H), 3.22 (s, 3H), 2.80 – 2.72 (m, 2H), 2.28 (d, *J* = 14.6 Hz, 1H), 2.05 (s, 2H), 1.98 (d, *J* = 11.5 Hz, 1H), 1.87 (p, *J* = 6.9 Hz, 2H), 1.78 (s, 2H), 1.62 – 1.48 (m, 6H), 1.43 – 1.19 (m, 6H), 0.93 (dd, *J* = 11.0, 3.4 Hz, 1H), 0.85 (d, *J* = 6.4 Hz, 6H). LCMS (Table SI-2, Method b) R_t = 1.91 min.; m/z = 886.6 [M+H$^+$].

2-((6aR,6bS,7S,8aS,8bS,10R,11aR,12aS,12bS)-7-Hydroxy-6a,8a-dimethyl-4-oxo-10-propyl-2,4,6a,6b,7,8,8a,8b,11a,12,12a,12b-dodecahydro-1H-naphtho[2',1':4,5]indeno[1,2-d][1,3]dioxol-8b-yl)-2-oxoethyl (3-(((((4-((S)-2-((S)-2-(6-(2,5-dioxo-2,5-dihydro-1H-pyrrol-1-yl)hexanamido)-3-methylbutanamido)propanamido)benzyl)oxy)carbonyl)amino)methyl)-6-(2,5,8,11,14,17-hexaoxaicosan-20-yl)pyridin-2-yl)(methyl)carbamate (DL16)

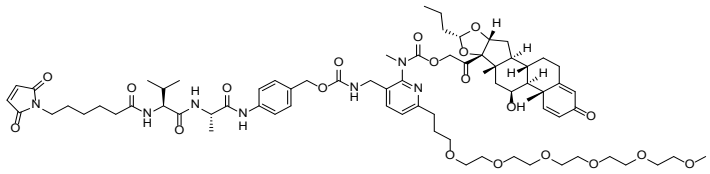

2-((6aR,6bS,7S,8aS,8bS,10R,11aR,12aS,12bS)-7-Hydroxy-6a,8a-dimethyl-4-oxo-10-propyl-2,4,6a,6b,7,8,8a,8b,11a,12,12a,12b-dodecahydro-1H-naphtho[2',1':4,5]indeno[1,2-d][1,3]dioxol-8b-yl)-2-oxoethyl (3-(aminomethyl)-6-(2,5,8,11,14,17-hexaoxaicosan-20-yl)pyridin-2-yl)(methyl)carbamate hydrochloride (**Bud-RG-9**) (0.077 g, 0.084 mmol) was added to a 0 °C solution of 4-((S)-2-((S)-2-(6-(2,5-dioxo-2,5-dihydro-1H-pyrrol-1-yl)hexanamido)-3-methylbutanamido)propanamido)benzyl (4-nitrophenyl) carbonate (**20b**) (0.060 g, 0.084 mmol) and DIPEA (0.060 mL, 0.335 mmol) in DMF (1.5 mL). The reaction mixture was stirred at room temperature for 30 min. Removed solvent under reduced pressure. Dissolved in DMF (2 mL) for purification by reverse phase prep HPLC eluting with a gradient of

40-85% CH_3CN/water (0.1% formic acid) over 20 min (21.2 x 250 mm). Product-containing fractions were lyophilized to give 2-((6aR,6bS,7S,8aS,8bS,10R,11aR,12aS,12bS)-7-hydroxy-6a,8a-dimethyl-4-oxo-10-propyl-2,4,6a,6b,7,8,8a,8b,11a,12,12a,12b-dodecahydro-1H-naphtho[2',1':4,5]indeno[1,2-d][1,3]dioxol-8b-yl)-2-oxoethyl (3-(((((4-((S)-2-((S)-2-(6-(2,5-dioxo-2,5-dihydro-1H-pyrrol-1-yl)hexanamido)-3-methylbutanamido)propanamido)benzyl)oxy)carbonyl)amino)methyl)-6-(2,5,8,11,14,17-hexaoxaicosan-20-yl)pyridin-2-yl)(methyl)carbamate (**DL16**) (0.041 g, 35% yield). ^{1}H NMR (400 MHz, DMSO-*d*6) δ 9.89 (s, 1H), 8.10 (d, *J* = 7.0 Hz, 1H), 7.76 (d, *J* = 8.6 Hz, 1H), 7.62 (s, 2H), 7.57 (d, *J* = 8.2 Hz, 2H), 7.29 (d, *J* = 10.2 Hz, 2H), 7.28 – 7.18 (m, 2H), 6.97 (s, 2H), 6.14 (dd, *J* = 10.1, 1.8 Hz, 1H), 5.89 (d, *J* = 1.8 Hz, 1H), 4.94 (s, 2H), 4.78 (s, 3H), 4.68 (s, 1H), 4.62 (s, 1H), 4.37 (t, *J* = 7.1 Hz, 1H), 4.27 (s, 1H), 4.15 (dd, *J* = 8.6, 6.8 Hz, 1H), 3.52 – 3.44 (m, 19H), 3.43 – 3.38 (m, 4H), 3.35 (t, *J* = 7.0 Hz, 2H), 3.21 (s, 2H), 3.20 – 3.11 (m, 3H), 2.71 (t, *J* = 7.7 Hz, 2H), 2.27 (d, *J* = 12.7 Hz, 1H), 2.22 – 2.04 (m, 2H), 1.96 (p, *J* = 6.6 Hz, 1H), 1.89 – 1.81 (m, 2H), 1.78 (s, 2H), 1.52 (s, 7H), 1.55 – 1.40 (m, 4H), 1.36 (s, 3H), 1.29 (d, *J* = 7.1 Hz, 3H), 1.17 (p, *J* = 7.6 Hz, 2H), 1.05 – 0.87 (m, 3H), 0.89 – 0.77 (m, 13H). LCMS (Table SI-2, Method b) Rt = 2.34 min; m/z = 1399.0 [M+H$^+$].

(9H-Fluoren-9-yl)methyl ((S)-1-(((S)-1-((4-(hydroxymethyl)phenyl)amino)-1-oxopropan-2-yl)amino)-1-oxopropan-2-yl)carbamate

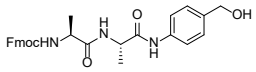

A 100 mL round bottom flask was charged with Fmoc-Ala-Ala-OH (Chem-Impex, 1.43 g, 3.74 mmol), 4-aminobenzyl alcohol (0.5061 g, 4.11 mmol), EEDQ (1.18 g, 4.77 mmol) and THF (18 mL). The resulting solution was stirred at room temperature overnight. Diluted with THF (24 mL) and filtered. Used additional portions of THF (2 x 12 mL) to wash the filter cake, which was dried in the vacuum oven over night. (9H-Fluoren-9-yl)methyl ((S)-1-(((S)-1-((4-(hydroxymethyl)phenyl)amino)-1-oxopropan-2-yl)amino)-1-oxopropan-2-yl)carbamate (1.28 g, 2.63 mmol, 70% yield) was isolated as a white solid. ^{1}H NMR (400 MHz, DMSO-*d*6) δ 9.85 (s, 1H), 8.06 (d, J = 7.3 Hz, 1H), 7.85 (d, J = 7.5 Hz, 2H), 7.68 (t, J = 8.2 Hz, 2H), 7.54 – 7.47 (m, 3H), 7.42 – 7.34 (m, 2H), 7.29 (td, J = 7.5, 1.2 Hz, 2H), 7.23 – 7.17 (m, 2H), 5.08 (t, J = 5.7 Hz, 1H), 4.38 (dd, J = 14.0, 6.4 Hz, 3H), 4.27 – 4.14 (m, 3H), 4.06 (p, J = 7.2 Hz, 1H), 1.27 (d, J = 7.0 Hz, 3H), 1.20 (d, J = 7.1 Hz, 3H). LCMS (Table SI-2, Method s) Rt = 0.86 min; m/z = 488.1 [M+H$^+$].

(S)-2-Amino-N-((S)-1-((4-(hydroxymethyl)phenyl)amino)-1-oxopropan-2-yl)propanamide

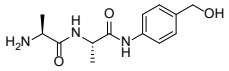

Piperidine (26.5 g, 312 mmol) was added to a 0 °C solution of (9H-fluoren-9-yl)methyl ((S)-1-(((S)-1-((4-(hydroxymethyl)phenyl)amino)-1-oxopropan-2-yl)amino)-1-oxopropan-2-yl)carbamate (20 g, 38 mmol) in DMF (200 mL). The mixture was stirred at 20 °C for 2 h. The reaction mixture was concentrated under reduced pressure and the residue was dissolved in methanol (100 mL) and then was filtered. The filtrate was concentrated under reduced pressure and washed with a mixture of MTBE and EtOAc (3:1, 300 mL) to obtain (S)-2-amino-*N*-((S)-1-((4-(hydroxymethyl)phenyl)amino)-1-oxopropan-2-yl)propanamide (10 g, 35.8 mmol, 92% yield) as a white solid. ^{1}H NMR (400 MHz, CD_3OD) 7.53 δ (d, J = 8.4 Hz, 2H), 7.30 (d, J = 8.4 Hz, 2H), 4.55 (s, 2H), 4.48 (q, J = 7.1 Hz, 1H), 3.54 - 3.43 (m, 1H), 1.44 (d, J = 7.1 Hz, 3H), 1.30 (d, J = 6.6 Hz, 3H).

3-(2,5-Dioxo-2,5-dihydro-1H-pyrrol-1-yl)-N-((S)-1-(((S)-1-((4-(hydroxymethyl)phenyl)amino)-1-oxopropan-2-yl)amino)-1-oxopropan-2-yl)propanamide

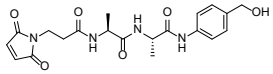

2,5-Dioxopyrrolidin-1-yl 3-(2,5-dioxo-2,5-dihydro-1H-pyrrol-1-yl)propanoate (15g, 53.8 mmol) was added to a 0 °C solution of (S)-2-amino-*N*-((S)-1-((4-(hydroxymethyl)phenyl)amino)-1-oxopropan-2-yl)propanamide (10 g, 25.8 mmol) in DMF (100 mL). The mixture was warmed to room temperature and stirred for 2 h. The reaction was concentrated under reduced pressure and the residue was washed with DCM (200 mL) to obtain 3-(2,5-dioxo-2,5-dihydro-1H-pyrrol-1-yl)-*N*-((S)-1-(((S)-1-((4-(hydroxymethyl)phenyl)amino)-1-oxopropan-2-yl)amino)-1-oxopropan-2-yl)propanamide (10 g, 22.90 mmol, 65% yield) as a white solid. ^{1}H NMR (400 MHz, DMSO-*d*6) δ 9.75 (s, 1H), 8.21 (d, J = 7.1 Hz, 1H), 8.08 (d, J = 7.5 Hz, 1H), 7.56 (d, J = 8.4 Hz, 2H), 7.23 (d, J = 7.9 Hz, 2H), 7.00 (s, 2H), 5.09 (t, J = 5.7 Hz, 1H), 4.43 (d, J = 5.7 Hz, 2H), 4.37 (t, J = 7.3 Hz, 1H), 4.26 - 4.19 (m, 1H), 3.61 (t, J = 7.3 Hz, 2H), 2.41 (t, J = 7.3 Hz, 2H), 1.30 (d, J = 7.1 Hz, 3H), 1.18 (d, J = 7.1 Hz, 3H). LCMS (Table SI-2, method p) Rt = 2.052 min; m/z = 439.1 [M+Na$^+$].

4-((S)-2-((S)-2-(3-(2,5-Dioxo-2,5-dihydro-1H-pyrrol-1-yl)propanamido)propanamido)propanamido)benzyl (4-nitrophenyl) carbonate (**20f**)

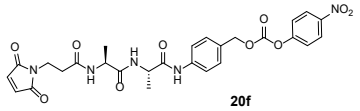

20f

A mixture of DIPEA (0.8 mL, 4.49 mmol), bis(4-nitrophenyl) carbonate (1.366 g, 4.49 mmol), 3-(2,5-dioxo-2,5-dihydro-1H-pyrrol-1-yl)-*N*-((S)-1-(((S)-1-((4-(hydroxymethyl)phenyl)amino)-1-oxopropan-2-yl)amino)-1-oxopropan-2-yl)propanamide (1.7 g, 4.08 mmol) in DMF (20 mL) was stirred at 25 °C for 2 h. The reaction was diluted with DCM (200 mL), washed with a sat. aq. solution of NaCl (100 mL), dried (Na_2SO_4) and solvent was removed to give a yellow oil. Purification by chromatography (silica) eluting with 10% MeOH/DCM gave (S)-2-((S)-2-(3-(2,5-dioxo-2,5-dihydro-1H-pyrrol-1-yl)propanamido)propanamido)propanamido)benzyl (4-nitrophenyl) carbonate (**20f**) (1.27 g, 2.18 mmol, 54% yield) as a white solid. ^{1}H NMR (400 MHz, DMSO-*d*6) δ 9.88 (s, 1H), 8.29 (d, J=9.3 Hz, 2H), 8.19 (d, J=7.1 Hz, 1H), 8.10 (d, J=7.1 Hz, 1H), 7.65 (d, J=8.4 Hz, 2H), 7.54 (d, J=8.8 Hz, 2H), 7.39 (d, J=8.4 Hz, 2H), 6.98 (s, 2H), 5.22 (s, 2H), 4.35 (quin, J=7.2 Hz, 1H), 4.21 (quin, J=6.9 Hz, 1H), 3.59 (t, J=7.3 Hz, 2H), 2.38 (t, J=7.3 Hz, 2H), 1.29 (d, J=7.1 Hz, 3H), 1.16 (d, J=7.1 Hz, 3H). LCMS (Table SI-2, method p) Rt = 2.96 min; m/z = 604.2 [M+Na$^+$].

2-((6aR,6bS,7S,8aS,8bS,10R,11aR,12aS,12bS)-7-Hydroxy-6a,8a-dimethyl-4-oxo-10-propyl-2,4,6a,6b,7,8,8a,8b,11a,12,12a,12b-dodecahydro-1H-naphtho[2',1':4,5]indeno[1,2-d][1,3]dioxol-8b-yl)-2-oxoethyl (3-(((((4-((S)-2-((S)-2-(3-(2,5-dioxo-2,5-dihydro-1H-pyrrol-1-yl)propanamido)propanamido)propanamido)benzyl)oxy)carbonyl)amino)methyl)-6-(2,5,8,11,14,17-hexaoxaicosan-20-yl)pyridin-2-yl)(methyl)carbamate (**DL23**)

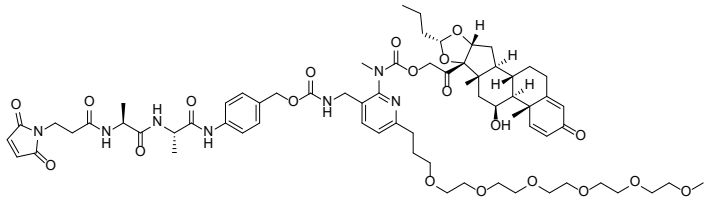

DIPEA (0.060 mL, 0.344 mmol) was added drop-wise to a room temperature solution of 2-((6aR,6bS,7S,8aS,8bS,10R,11aR,12aS,12bS)-7-hydroxy-6a,8a-dimethyl-4-oxo-10-propyl-2,4,6a,6b,7,8,8a,8b,11a,12,12a,12b-dodecahydro-1H-naphtho[2',1':4,5]indeno[1,2-d][1,3]dioxol-8b-yl)-2-oxoethyl (3-(aminomethyl)-6-(2,5,8,11,14,17-hexaoxaicosan-20-yl)pyridin-2-yl)(methyl)carbamate hydrochloride (**Bud-RG-9**) (0.159 g, 0.172 mmol) and 4-((S)-2-((S)-2-(3-(2,5-dioxo-2,5-dihydro-1H-pyrrol-1-yl)propanamido)propanamido)propanamido)benzyl (4-nitrophenyl) carbonate (0.100 g, 0.172 mmol) in DMF (1.8 mL). The reaction stirred at ambient temperature for 45 min, and then solvent was removed under reduced pressure. Purified by reverse phase prep HPLC eluting with a gradient of 35 to 95% MeCN/water (0.1% formic acid) over 12 minutes. The desired fractions were combined and lyophilized to give the 2-((6aR,6bS,7S,8aS,8bS,10R,11aR,12aS,12bS)-7-hydroxy-6a,8a-dimethyl-4-oxo-10-propyl-2,4,6a,6b,7,8,8a,8b,11a,12,12a,12b-dodecahydro-1H-naphtho[2',1':4,5]indeno[1,2-d][1,3]dioxol-8b-yl)-2-oxoethyl (3-(((((4-((S)-2-((S)-2-(3-(2,5-dioxo-2,5-dihydro-1H-pyrrol-1-yl)propanamido)propanamido)propanamido)benzyl)oxy)carbonyl)amino)methyl)-6-(2,5,8,11,14,17-hexaoxaicosan-20-yl)pyridin-2-yl)(methyl)carbamate (**DL23**) (0.075 g, 29% yield) as a white powder. ^{1}H NMR (400 MHz, DMSO-*d*6) δ 9.82 (s, 1H), 8.19 (d, J = 6.9 Hz, 1H), 8.07 (d, J = 7.2 Hz, 1H), 7.63 (t, J = 9.6 Hz, 3H), 7.30 (dd, J = 9.3, 6.1 Hz, 3H), 7.23 (d, J = 7.9 Hz, 1H), 6.99 (s, 2H), 6.16 (dt, J = 10.1, 1.6 Hz, 1H), 5.94 - 5.89 (m, 1H), 4.97 (s, 3H), 4.87 - 4.73 (m, 2H), 4.67 (d, J = 24.0 Hz, 2H), 4.42 - 4.33 (m, 1H), 4.29 (q, J = 8.3, 5.9 Hz, 2H), 4.22 (q, J = 7.0 Hz, 1H), 3.62 (t, J = 7.3 Hz, 2H), 3.54 - 3.46 (m, 19H), 3.44 - 3.39 (m, 4H), 3.24 - 3.21 (m, 3H), 3.21 - 3.16 (m, 1H), 2.73 (t, J = 7.7 Hz, 2H), 2.41 (dd, J = 8.0, 6.5 Hz, 2H), 2.34 - 2.25 (m, 1H), 2.13 - 1.94 (m, 2H), 1.92 - 1.84 (m, 2H), 1.80 (s, 2H), 1.61 - 1.48 (m, 6H), 1.38 (d, J = 2.3 Hz, 4H), 1.31 (d, J = 7.1 Hz, 5H), 1.19 (d, J = 7.1 Hz, 3H), 1.02 - 0.90 (m, 2H), 0.85 (tt, J = 9.3, 4.5 Hz, 7H). LCMS (Table SI-2, method j) Rt = 2.16 min; m/z = 1329.3 [M+H^{+}]. HRMS-ESI (positive ionization) m/z [M+H^{+}] calcd for $C_{68}H_{94}N_7O_{20}$, 1328.6553; found, 1328.6553.

General Cysteine Conjugation Protocol

Prepared an approximately 10 mg/mL solution of the desired antibody in PBS buffer (pH 7.4) as well as a separate 10 mM TCEP solution in PBS (Pierce Bond-Breaker, cat. 77720). Antibodies were then partially reduced by adding approximately two molar equivalents of 10 mM TCEP, briefly mixing, and incubating for 60 min at 37 °C. DMSO was then added to the partially reduced antibodies in sufficient quantity to 15% total DMSO. For the conjugations, 8 molar equivalents of a 10 mM drug-linker (**DL**) solutions were then added and incubated for 30 min at room temperature. Excess combo and DMSO were then removed using NAP-5 desalting columns (GE Healthcare, cat. 17-0853-02) previously equilibrated with PBS buffer, pH 7.4. Desalted samples were then analyzed by size exclusion chromatography (SEC), hydrophobic interaction chromatography (HIC), and reduced mass spectrometry.

Maleimide Hydrolysis

Hydrolysis of the succinimide ring of the ADCs was accomplished by incubating the ADCs at an elevated pH. Arginine buffer (0.7 M), pH 9.0 solution was prepared and added to the ADC in PBS buffer to bring the total arginine concentration to 50 mM (pH ~ 8.9). The material was then incubated at 25 °C for 72

hours. Hydrolysis of the succinimide ring was then confirmed by reduced mass spectrometry, after which, hydrolysis was quenched with the addition of a 0.1 M acetic acid solution to 12.5 mM total acetic acid (pH ~ 7.1).

ADC Analytical Procedures

Hydrophobic Interaction Chromatography. ADCs were profiled by hydrophobic interaction chromatography (HIC) and mass spectroscopy (MS) to determine degree of conjugation and to calculate approximate drug-to-antibody ratios (DARs). Briefly, 100 μg of the ADCs was dissolved in 25 mM sodium phosphate buffer and loaded onto an Ultimate 3000 Dual LC system (Thermo Scientific) equipped with a 4.6 X 35 mm butyl-NPR column (Tosoh Bioscience, cat. 14947). ADCs were loaded onto the column equilibrated in 100% buffer A and eluted using a linear gradient from 100% buffer A to 100% buffer B over 12 min at 0.8 mL/min, where buffer A is 25 mM sodium phosphate, 1.5 M ammonium sulfate, pH 7.25 and buffer B is 25 mM sodium phosphate, 20% isopropanol, pH 7.25. The DAR was determined by taking the sum of each peak percent area multiplied by their corresponding drug load and dividing the weighted sum by 100.

Size Exclusion Chromatography. Size distributions of the ADCs were profiled by size exclusion chromatography (SEC) using an Ultimate 3000 Dual LC system (Thermo Scientific) equipped with a 7.8 X 300 mm TSK-gel 3000SW_{XL} column (Tosoh Bioscience, cat. 08541). 20 ug of each of the ADCs were dissolved in PBS buffer and were loaded onto the column and eluted over 17 min using an isocratic gradient at 1mL/min of 100 mM sodium sulfate, 100 mM sodium phosphate, pH 6.8 at 0.8 mL/min.

K562 GRE (PGL4.36-Promega) Reporter Assay

K562 parental GRE and K562 mCD19 GRE cells were plated onto 96 well tissue culture treated white plates (Costar: 3917) at 50,000 cells per well in 50 µL of assay medium (RPMI, 1% CSFBS, 1% L-glutamine, 1% Na Pyruvate and 1% MAEE). The cells were treated with 25 µL of 3x serial diluted murine CD19 antibody-drug conjugates in assay medium, steroid compound or media alone and incubated for 48 h at 37° C, 5% CO_2. After 48 h incubation, cells were treated with 75 µL of Dual-Glo Luciferase Assay System (Promega-E2920) for 10 min and analyzed for luminescence using the TopCount (PerkinElmer).

Data shows that higher luminescence is observed in the cells expressing CD19 demonstrating that the CD19 ADC is binding, internalizing and releasing the steroid intracellularly. The lack of efficacy in the cells that do not express CD19 demonstrates that efficacy in the cells expressing CD19 is not due to extracellular release of small molecule and subsequent distribution into the cell.

Animal Welfare

All animal experiments performed in the work were conducted in compliance with institutional guidelines.

Associated Content

Supporting Information

General experimental information. Synthetic procedures for all compounds. NMR and HPLC data for drug-linkers. Experimental protocols for budesonide release experiments and determination of rate constants. GRE reporter data for (*R*)-budesonide (**6**), (*S*)-budesonide, and triamcinolone acetonide.

Stability data for **ADC23** in buffer and plasma. Protocol for NP-CGG immunized mouse model. HIC and SEC data for ADCs. Reduced mass spec data for ADC23 and ADC25.

Author Information

Corresponding Author

* christopher.marvin@abbvie.com

Author Contributions

The manuscript was written through contributions of all authors. All authors have given approval to the final version of the manuscript.

Disclosures

CCM, ADH, MM, TAD, MEH, MMF, AB, LW, LW, AH, YJ, and YT are employees of AbbVie. TRV and JZO were employees of AbbVie at the time of the study. The design, study conduct, and financial support for this research were provided by AbbVie. AbbVie participated in the interpretation of data, review, and approval of the publication.

Acknowledgments

AbbVie employees Jan Waters and Kimberly Yach (Structural Chemistry group) are thanked for compound characterization support. We thank Chau-Wen Chou from the Proteomics and Mass Spectrometry Core Facility at the University of Georgia (supported by NIH grant no. S10 OD025118) for high resolution mass spectrometry analysis. AbbVie paid for HRMS analysis on a per sample basis.

Abbreviations

ADC: antibody-drug conjugate; ACN: acetonitrile; Boc2O: di-tert-butyl dicarbonate; cLogP: calculated logP; DAR: drug to antibody ratio; DCM: dichloromethane; DIPEA: N,N-diisopropylethylamine; DMAP: 4-dimethylaminopyridine; DMF: N,N-dimethylformamide; DMSO: dimethyl sulfoxide; EEDQ: N-ethoxycarbonyl-2-ethoxy-1,2-dihydroquinoline; EtOAc: ethyl acetate; Fmoc: fluorenylmethyloxycarbonyl; GR: glucocorticoid receptor; GRE: Glucocorticoid response element; GRM: glucocorticoid receptor modulator; HATU: 1-[bis(dimethylamino)methylene]-1H-1,2,3-triazolo[4,5-b]pyridinium 3-oxid hexafluorophosphate; HCTU: O-(1H-6-chlorobenzotriazole-1-yl)-1,1,3,3-tetramethyluronium hexafluorophosphate; HIC: Hydrophobic interaction chromatography; HOBT: hydroxybenzotriazole; HPLC: High performance liquid chromatography; HRMS: high resolution mass spectrometry; IPA: isopropyl alcohol; LCMS: liquid chromatography mass spectrometry; mAb: monoclonal antibody; MTBE: tert-butyl methyl ether; MS: mass spectrometry; NMP: N-methyl-2-pyrrolidinone; NMR: nuclear magnetic resonance; PABC: para-amino benzylic carbamate; SEC: size exclusion chromatography; SAR: structure-activity relationship; TCEP: tris(2-carboxyethyl)phosphine; TEA: triethylamine; tetX: tetanus toxin; TFA: trifluoroacetic acid; THF: tetrahydrofuran; TNF: Tumor necrosis factor.

References

(1) Goundry, W. R. F.; Parker, J. S. Payloads for Antibody–Drug Conjugates. *Org. Process. Res. Dev.* **2022**, *26*, 2121–2123. https://doi.org/10.1021/acs.oprd.2c00227.

(2) Hobson, A. D.; McPherson, M. J.; Waegell, W.; Goess, C. A.; Stoffel, R. H.; Li, X.; Zhou, J.; Wang, Z.; Yu, Y.; Hernandez, A.; Bryant, S. H.; Mathieu, S. L.; Bischoff, A. K.; Fitzgibbons, J.; Pawlikowska, M.; Puthenveetil, S.; Santora, L. C.; Wang, L.; Wang, L.; Marvin, C. C.; Hayes, M. E.; Shrestha, A.; Sarris, K. A.; Li, B. Design and Development of Glucocorticoid Receptor Modulators as Immunology Antibody–Drug Conjugate Payloads. *J. Med. Chem.* **2022**, *65*, 4500–4533. https://doi.org/10.1021/acs.jmedchem.1c02099.

(3) Hobson, A. D.; McPherson, M. J.; Hayes, M. E.; Goess, C.; Li, X.; Zhou, J.; Wang, Z.; Yu, Y.; Yang, J.; Sun, L.; Zhang, Q.; Qu, P.; Yang, S.; Hernandez, A.; Bryant, S. H.; Mathieu, S. L.; Bischoff, A. K.; Fitzgibbons, J.; Santora, L. C.; Wang, L.; Wang, L.; Fettis, M. M.; Li, X.; Marvin, C. C.; Wang, Z.; Patel, M. V.; Schmidt, D. L.; Li, T.; Randolph, J. T.; Henry, R. F.; Graff, C.; Tian, Y.; Aguirre, A. L.; Shrestha, A. Discovery of ABBV-3373, an Anti-TNF Glucocorticoid Receptor Modulator Immunology Antibody Drug Conjugate. *J. Med. Chem.* **2022**, *65*, 15893–15934. https://doi.org/10.1021/acs.jmedchem.2c01579.

(4) Teitelbaum, A. M.; Meissner, A.; Harding, R. A.; Wong, C. A.; Aldrich, C. C.; Remmel, R. P. Synthesis, PH-Dependent, and Plasma Stability of Meropenem Prodrugs for Potential Use against Drug-Resistant Tuberculosis. *Bioorg. Med. Chem.* **2013**, *21*, 5605–5617. https://doi.org/10.1016/j.bmc.2013.05.024.

(5) Govindan, S. V.; Cardillo, T. M.; Rossi, E. A.; Trisal, P.; McBride, W. J.; Sharkey, R. M.; Goldenberg, D. M. Improving the Therapeutic Index in Cancer Therapy by Using Antibody–Drug Conjugates Designed with a Moderately Cytotoxic Drug. *Mol Pharmaceut* **2015**, *12*, 1836–1847. https://doi.org/10.1021/mp5006195.

(6) Goldenberg, D. M.; Sharkey, R. M. Sacituzumab Govitecan, a Novel, Third-Generation, Antibody-Drug Conjugate (ADC) for Cancer Therapy. *Expert Opin. Biol. Ther.* **2020**, 1–15. https://doi.org/10.1080/14712598.2020.1757067.

(7) Santi, D. V.; Cabel, L.; Bidard, F.-C. Does Sacituzumab-Govitecan Act as a Conventional Antibody Drug Conjugate (ADC), a Prodrug of SN-38 or Both? *Ann. Transl. Med.* 2021, *9* (14), 1113. https://dx.doi.org/10.21037/atm-21-1103.

(8) Graverson, J. H.; Svendsen, P.; Christensen, P. A.; Maniecki, M. B.; Moestrup, S. K.; Mollerm H, J.; Anton, G. Conjugates Targeting the CD163 Receptor, WO2011 039510 A2.

(9) Graversen, J. H.; Svendsen, P.; Dagnæs-Hansen, F.; Dal, J.; Anton, G.; Etzerodt, A.; Petersen, M. D.; Christensen, P. A.; Møller, H. J.; Moestrup, S. K. Targeting the Hemoglobin Scavenger Receptor CD163 in Macrophages Highly Increases the Anti-Inflammatory Potency of Dexamethasone. *Mol. Ther.* **2012**, *20*, 1550–1558. https://doi.org/10.1038/mt.2012.103.

(10) Granfeldt, A.; Hvas, C. L.; Graversen, J. H.; Christensen, P. A.; Petersen, M. D.; Anton, G.; Svendsen, P.; Sølling, C.; Etzerodt, A.; Tønnesen, E.; Moestrup, S. K.; Møller, H. J. Targeting Dexamethasone to Macrophages in a Porcine Endotoxemic Model. *Crit. Care Med.* **2013**, *41* (11), e309–e318. https://doi.org/10.1097/ccm.0b013e31828a45ef.

(11) Svendsen, P.; Graversen, J. H.; Etzerodt, A.; Hager, H.; Røge, R.; Grønbæk, H.; Christensen, E. I.; Møller, H. J.; Vilstrup, H.; Moestrup, S. K. Antibody-Directed Glucocorticoid Targeting to CD163 in M2-Type Macrophages Attenuates Fructose-Induced Liver Inflammatory Changes. *Mol. Ther. Methods Clin. Dev.* **2017**, *4*, 50–61. https://doi.org/10.1016/j.omtm.2016.11.004.

(12) Everts, M.; Kok, R. J.; Ásgeirsdóttir, S. A.; Melgert, B. N.; Moolenaar, T. J. M.; Koning, G. A.; Luyn, M. J. A. van; Meijer, D. K. F.; Molema, G. Selective Intracellular Delivery of Dexamethasone into Activated Endothelial Cells Using an E-Selectin-Directed Immunoconjugate. *J. Immunol.* **2002**, *168* (2), 883–889. https://doi.org/10.4049/jimmunol.168.2.883.

(13) Ogitani, Y.; Aida, T.; Hagihara, K.; Yamaguchi, J.; Ishii, C.; Harada, N.; Soma, M.; Okamoto, H.; Oitate, M.; Arakawa, S.; Hirai, T.; Atsumi, R.; Nakada, T.; Hayakawa, I.; Abe, Y.; Agatsuma, T. DS-8201a, A Novel HER2-Targeting ADC with a Novel DNA Topoisomerase I Inhibitor, Demonstrates a Promising Antitumor Efficacy with Differentiation from T-DM1. *Clin. Cancer. Res.* **2016**, *22* (20), 5097–5108. https://doi.org/10.1158/1078-0432.ccr-15-2822.

(14) Nakada, T.; Masuda, T.; Naito, H.; Yoshida, M.; Ashida, S.; Morita, K.; Miyazaki, H.; Kasuya, Y.; Ogitani, Y.; Yamaguchi, J.; Abe, Y.; Honda, T. Novel Antibody Drug Conjugates Containing Exatecan Derivative-Based Cytotoxic Payloads. *Bioorg. Med. Chem. Lett.* **2016**, *26*, 1542–1545. https://doi.org/10.1016/j.bmcl.2016.02.020.

(15) Kern, J. C.; Cancilla, M.; Dooney, D.; Kwasnjuk, K.; Zhang, R.; Beaumont, M.; Figueroa, I.; Hsieh, S.; Liang, L.; Tomazela, D.; Zhang, J.; Brandish, P. E.; Palmieri, A.; Stivers, P.; Cheng, M.; Feng, G.; Geda, P.; Shah, S.; Beck, A.; Bresson, D.; Firdos, J.; Gately, D.; Knudsen, N.; Manibusan, A.; Schultz, P. G.; Sun, Y.; Garbaccio, R. M. Discovery of Pyrophosphate Diesters as Tunable, Soluble, and Bioorthogonal Linkers for Site-Specific Antibody–Drug Conjugates. *J. Am. Chem. Soc.* **2016**, *138*, 1430–1445. https://doi.org/10.1021/jacs.5b12547.

(16) Kern, J. C.; Dooney, D.; Zhang, R.; Liang, L.; Brandish, P. E.; Cheng, M.; Feng, G.; Beck, A.; Bresson, D.; Firdos, J.; Gately, D.; Knudsen, N.; Manibusan, A.; Sun, Y.; Garbaccio, R. M. Novel Phosphate Modified Cathepsin B Linkers: Improving Aqueous Solubility and Enhancing Payload Scope of ADCs. *Bioconjug. Chem.* **2016**, *27*, 2081–2088. https://doi.org/10.1021/acs.bioconjchem.6b00337.

(17) Brandish, P. E.; Palmieri, A.; Antonenko, S.; Beaumont, M.; Benso, L.; Cancilla, M.; Cheng, M.; Fayadat-Dilman, L.; Feng, G.; Figueroa, I.; Firdos, J.; Garbaccio, R.; Garvin-Queen, L.; Gately, D.; Geda, P.; Haines, C.; Hseih, S.; Hodges, D.; Kern, J.; Knudsen, N.; Kwasnjuk, K.; Liang, L.; Ma, H.; Manibusan, A.; Miller, P. L.; Moy, L. Y.; Qu, Y.; Shah, S.; Shin, J. S.; Stivers, P.; Sun, Y.; Tomazela, D.; Woo, H. C.; Zaller, D.; Zhang, S.; Zhang, Y.; Zielstorff, M. Development of Anti-CD74 Antibody–Drug Conjugates to Target Glucocorticoids to Immune Cells. *Bioconjug. Chem.* **2018**, *29*, 2357–2369. https://doi.org/10.1021/acs.bioconjchem.8b00312.

(18) Elgersma, R. C.; Coumans, R. G. E.; Huijbregts, T.; Menge, W. M. P. B.; Joosten, J. A. F.; Spijker, H. J.; Groot, F. M. H. de; Lee, M. M. C. van der; Ubink, R.; Dobbelsteen, D. J. van den; Egging, D. F.; Dokter, W. H. A.; Verheijden, G. F. M.; Lemmens, J. M.; Timmers, C. M.; Beusker, P. H. Design, Synthesis, and Evaluation of Linker-Duocarmycin Payloads: Toward Selection of HER2-Targeting Antibody–Drug Conjugate SYD985. *Mol. Pharmaceut.* **2015**, *12* (6), 1813–1835. https://doi.org/10.1021/mp500781a.

(19) Grier, K. E.; Hansen, A. H.; Haxvig, C. S.; Li, X.; Krigslund, O.; Behrendt, N.; Engelholm, L. H.; Rossi, F.; Sousa, B. C.; Harradence, G. J.; Camper, N.; Qvortrup, K. M. Targeted Delivery of Alcohol-Containing Payloads with Antibody-Drug Conjugates. *Chem. Commun.* **2023**. https://doi.org/10.1039/d3cc01596c.

(20) Corso, A. D.; Frigoli, M.; Prevosti, M.; Mason, M.; Bucci, R.; Belvisi, L.; Pignataro, L.; Gennari, C. Advanced Pyrrolidine-Carbamate Self-Immolative Spacer with Tertiary Amine Handle Induces Superfast Cyclative Drug Release. *ChemMedChem* **2022**, *17* (15), e202200279. https://doi.org/10.1002/cmdc.202200279.

(21) Rosenberg, A. S. Effects of Protein Aggregates: An Immunologic Perspective. *AAPS J.* **2006**, *8* (3), E501–E507. https://doi.org/10.1208/aapsj080359.

(22) Wang, K.; Wei, G.; Liu, D. CD19: A Biomarker for B-cell Development, Lymphoma Diagnosis and Therapy. *Exp. Hematol. Oncol.* **2012**, *1* (1), 36. https://doi.org/10.1186/2162-3619-1-36.

(23) Li, X.; Ding, Y.; Zi, M.; Sun, L.; Zhang, W.; Chen, S.; Xu, Y. CD19, from Bench to Bedside. *Immunol. Lett.* **2017**, *183*, 86–95. https://doi.org/10.1016/j.imlet.2017.01.010.

(24) Hammer, O. CD19 as an Attractive Target for Antibody-Based Therapy. *MAbs.* **2012**, *4* (5), 571–577. https://doi.org/10.4161/mabs.21338.

(25) Milstien, S.; Cohen, L. A. Rate Acceleration by Stereopopulation Control: Models for Enzyme Action. *Proc. Nat. Acad. Sci.* **1970**, *67* (3), 1143–1147. https://doi.org/10.1073/pnas.67.3.1143.

(26) Milstien, S.; Cohen, L. A. Stereopopulation Control. I. Rate Enhancement in the Lactonizations of o-Hydroxyhydrocinnamic Acids. *J. Am. Chem. Soc.* **1972**, *94* (26), 9158–9165. https://doi.org/10.1021/ja00781a029.

(27) Levine, M. N.; Raines, R. T. Trimethyl Lock: A Trigger for Molecular Release in Chemistry, Biology, and Pharmacology. *Chem. Sci.* **2012**, *3* (8), 2412–2420. https://doi.org/10.1039/c2sc20536j.

(28) Xiao, D.; Luo, L.; Li, J.; Wang, Z.; Liu, L.; Xie, F.; Feng, J.; Zhou, X. Development of Bifunctional Anti-PD-L1 Antibody MMAE Conjugate with Cytotoxicity and Immunostimulation. *Bioorg. Chem.* **2021**, *116*, 105366. https://doi.org/10.1016/j.bioorg.2021.105366.

(29) Cahuzac, H.; Sallustrau, A.; Malgorn, C.; Beau, F.; Barbe, P.; Babin, V.; Dubois, S.; Palazzolo, A.; Thai, R.; Correia, I.; Lee, K. B.; Garcia-Argote, S.; Lequin, O.; Keck, M.; Nozach, H.; Feuillastre, S.; Ge, X.; Pieters, G.; Audisio, D.; Devel, L. Monitoring In Vivo Performances of Protein–Drug Conjugates Using Site-Selective Dual Radiolabeling and Ex Vivo Digital Imaging. *J. Med. Chem.* **2022**, *65* (9), 6953–6968. https://doi.org/10.1021/acs.jmedchem.2c00401.

(30) Aoyama, M.; Tada, M.; Yokoo, H.; Demizu, Y.; Ishii-Watabe, A. Fcγ Receptor-Dependent Internalization and Off-Target Cytotoxicity of Antibody-Drug Conjugate Aggregates. *Pharm. Res.* **2022**, *39* (1), 89–103. https://doi.org/10.1007/s11095-021-03158-x.

(31) Lyon, R. P.; Bovee, T. D.; Doronina, S. O.; Burke, P. J.; Hunter, J. H.; Neff-LaFord, H. D.; Jonas, M.; Anderson, M. E.; Setter, J. R.; Senter, P. D. Reducing Hydrophobicity of Homogeneous Antibody-Drug Conjugates Improves Pharmacokinetics and Therapeutic Index. *Nat. Biotechnol.* **2015**, *33* (7), 733–735. https://doi.org/10.1038/nbt.3212.

(32) Lyon, R.; Burke, P.; Hunter, J. Pegylated Drug-Linkers for Improved Ligand-Drug Conjugate Pharmacokinetics. WO2015 057699 A2.

(33) Burke, P. J.; Hamilton, J. Z.; Jeffrey, S. C.; Hunter, J. H.; Doronina, S. O.; Okeley, N. M.; Miyamoto, J. B.; Anderson, M. E.; Stone, I. J.; Ulrich, M. L.; Simmons, J. K.; McKinney, E. E.; Senter, P. D.; Lyon, R. P. Optimization of a PEGylated Glucuronide-Monomethylauristatin E Linker for Antibody–Drug Conjugates. *Mol. Cancer Ther.* **2017**, *16* (1), 116. https://doi.org/10.1158/1535-7163.MCT-16-0343.

(34) Jeffrey, S. C.; Nguyen, M. T.; Andreyka, J. B.; Meyer, D. L.; Doronina, S. O.; Senter, P. D. Dipeptide-Based Highly Potent Doxorubicin Antibody Conjugates. *Bioorg. Med. Chem. Lett.* **2006**, *16* (2), 358–362. https://doi.org/10.1016/j.bmcl.2005.09.081.

(35) Wang, Y.; Fan, S.; Zhong, W.; Zhou, X.; Li, S. Development and Properties of Valine-Alanine Based Antibody-Drug Conjugates with Monomethyl Auristatin E as the Potent Payload. *Int. J. Mol. Sci.* **2017**, *18* (9), 1860. https://doi.org/10.3390/ijms18091860.

(36) Miller, J. T.; Vitro, C. N.; Fang, S.; Benjamin, S. R.; Tumey, L. N. Enzyme-Agnostic Lysosomal Screen Identifies New Legumain-Cleavable ADC Linkers. *Bioconjug. Chem.* **2021**, *32* (4), 842–858. https://doi.org/10.1021/acs.bioconjchem.1c00124.

(37) Seeberger, S.; Griffin, R. J.; Hardcastle, I. R.; Golding, B. T. A New Strategy for the Synthesis of Taurine Derivatives Using the 'Safety-Catch' Principle for the Protection of Sulfonic Acids. *Org. Biomol. Chem.* **2007**, *5*, 132–138. https://doi.org/10.1039/b614333d.

(38) Shen, B.-Q.; Xu, K.; Liu, L.; Raab, H.; Bhakta, S.; Kenrick, M.; Parsons-Reponte, K. L.; Tien, J.; Yu, S.-F.; Mai, E.; Li, D.; Tibbitts, J.; Baudys, J.; Saad, O. M.; Scales, S. J.; McDonald, P. J.; Hass, P. E.; Eigenbrot, C.; Nguyen, T.; Solis, W. A.; Fuji, R. N.; Flagella, K. M.; Patel, D.; Spencer, S. D.; Khawli, L. A.; Ebens, A.; Wong, W. L.; Vandlen, R.; Kaur, S.; Sliwkowski, M. X.; Scheller, R. H.; Polakis, P.; Junutula, J. R. Conjugation Site Modulates the in Vivo Stability and Therapeutic Activity of Antibody-Drug Conjugates. *Nat. Biotechnol.* **2012**, *30* (2), 184–189. https://doi.org/10.1038/nbt.2108.

(39) Wei, C.; Zhang, G.; Clark, T.; Barletta, F.; Tumey, L. N.; Rago, B.; Hansel, S.; Han, X. Where Did the Linker-Payload Go? A Quantitative Investigation on the Destination of the Released Linker-Payload from an Antibody-Drug Conjugate with a Maleimide Linker in Plasma. *Anal. Chem.* **2016**, *88* (9), 4979–4986. https://doi.org/10.1021/acs.analchem.6b00976.

(40) Fontaine, S. D.; Reid, R.; Robinson, L.; Ashley, G. W.; Santi, D. V. Long-Term Stabilization of Maleimide–Thiol Conjugates. *Bioconjug. Chem.* **2015**, *26*, 145–152. https://doi.org/10.1021/bc5005262.

(41) Lyon, R. P.; Setter, J. R.; Bovee, T. D.; Doronina, S. O.; Hunter, J. H.; Anderson, M. E.; Balasubramanian, C. L.; Duniho, S. M.; Leiske, C. I.; Li, F.; Senter, P. D. Self-Hydrolyzing Maleimides Improve the Stability and Pharmacological Properties of Antibody-Drug Conjugates. *Nat. Biotechnol.* **2014**, *32* (10), 1059–1062. https://doi.org/10.1038/nbt.2968.

(42) Tumey, L. N.; Charati, M.; He, T.; Sousa, E.; Ma, D.; Han, X.; Clark, T.; Casavant, J.; Loganzo, F.; Barletta, F.; Lucas, J.; Graziani, E. I. Mild Method for Succinimide Hydrolysis on ADCs: Impact on ADC Potency, Stability, Exposure, and Efficacy. *Bioconjug. Chem.* **2014**, *25* (10), 1871–1880. https://doi.org/10.1021/bc500357n.

(43) Silva, N. S. D.; Klein, U. Dynamics of B-cells in Germinal Centres. *Nat. Rev. Immunol.* **2015**, *15* (3), 137–148. https://doi.org/10.1038/nri3804.

(44) Strehl, C.; Ehlers, L.; Gaber, T.; Buttgereit, F. Glucocorticoids—All-Rounders Tackling the Versatile Players of the Immune System. *Front. Immunol.* **2019**, *10*, 1744. https://doi.org/10.3389/fimmu.2019.01744.

(45) Yan, S.; Deng, X.; Wang, Q.; Sun, X.; Wei, W. Prednisone Treatment Inhibits the Differentiation of B Lymphocytes into Plasma Cells in MRL/MpSlac-Lpr Mice. *Acta Pharmacol. Sin.* **2015**, *36* (11), 1367–1376. https://doi.org/10.1038/aps.2015.76.

(46) Haneda, M.; Owaki, M.; Kuzuya, T.; Iwasaki, K.; Miwa, Y.; Kobayashi, T. Comparative Analysis of Drug Action on B-Cell Proliferation and Differentiation for Mycophenolic Acid, Everolimus, and Prednisolone. *J. Transplant.* **2014**, *97* (4), 405–412. https://doi.org/10.1097/01.tp.0000441826.70687.f6.

(47) Cupps, T. R.; Gerrard, T. L.; Falkoff, R. J.; Whalen, G.; Fauci, A. S. Effects of in Vitro Corticosteroids on B-cell Activation, Proliferation, and Differentiation. *J. Clin. Invest.* **1985**, *75* (2), 754–761. https://doi.org/10.1172/jci111757.